Structure-Activity Relationships of Novel Substituted Naphthalene Diimides as Anticancer Agents.[∞]

Andrea Milelli,[†] Vincenzo Tumiatti,[†§] Marialuisa Micco,[†] Guendalina Zuccari,[†] Lizzia Raffaghello,[#] Giovanna Bianchi,[#] Vito Pistoia,[#] Fernando Diaz,[&] Benet Pera,[&] Chiara Trigili,[&] Isabel Barasoain,[&] Caterina Musetti,[^] Marianna Toniolo,[^] Claudia Sissi,[^] Stefano Alcaro,[¶] Federica Moraca,[¶] Maddalena Zini,[‡] Claudio Stefanelli,[‡] and Anna Minarini[†*]

[†]*Department of Pharmaceutical Sciences, Alma Mater Studiorum, University of Bologna, Via Belmeloro 6, 40126 Bologna, Italy,*

[§]*Polo Scientifico-Didattico di Rimini, University of Bologna, 40100 Bologna, Italy*

[‡]*Department of Biochemistry "G. Moruzzi", University of Bologna, Via Irnerio 48, 40126 Bologna, Italy*

[^]*Department of Pharmaceutical Sciences, via Marzolo 5, 35131 Padova, Italy.*

[#]*Laboratory of Oncology, G. Gaslini Institute, L. Gaslini 5, 16147 Genova*

Italy

[&]*Centro de Investigaciones Biológicas, Consejo Superior de Investigaciones Científicas, Ramiro de Maeztu 9, 28040 Madrid, Spain*

[¶]*Dipartimento di Scienze della Salute, Università degli Studi "Magna Græcia" di Catanzaro, Campus Universitario "S. Venuta", 88100 Catanzaro, Italy*

[∞]Dedicated to Professor Carlo Melchiorre on the occasion of his retirement.

[*]Corresponding author: Anna Minarini, Department of Pharmaceutical Sciences, University of Bologna, Via Belmeloro 6, 40126 Bologna, Italy. Tel. +39-051-2099709. Fax: +39-051-2099734. E-mail: anna.minarini@unibo.it

[a]Abbreviations: DTP, Developmental Therapeutics Program; CD, circular dicroism; dsDNA, double strand DNA; ERK, extracellular signal regulated kinase; NAC, N-acetylcysteine; NCI, National Cancer Institute; NDI, 1,4,5,8-naphthalenetetracarboxylic diimide; PDB, Protein Data Bank; TRAP, telomeric repeat amplification protocol.

Abstract. Novel 1,4,5,8-naphthalentetracarboxylic diimide (NDI) derivatives were synthesized and evaluated for their antiproliferative activity on a wide number of tumor cell lines. The prototypes of the present series were derivatives **1** and **2** characterized by interesting biological profiles as anticancer agents. The present investigation expands on the study of structure-activity relationships of prototypes **1** and **2**, namely, the effect of the substituents on the phenyl ring. Derivatives **3**-**22**, characterized by a different substituent on the aromatic rings and/or a different chain length varying from two to three carbon units, were synthesized and evaluated for their cytostatic and cytotoxic activities. The most interesting compound was **20**, characterized by a linker of three methylene units and a 2,3,4-trimethoxy substituent on the two aromatic rings. It displayed antiproliferative activity in the submicromolar range, especially against colon and prostate cancer cell lines, the ability to inhibit Taq polymerase and telomerase, to trigger caspase activation by a possible oxidative mechanism, to downregulate ERK 2 protein and to inhibit ERKs phosphorylation, without acting directly on microtubules and tubuline. Its theoretical recognition against duplex and quadruplex DNA structures has been compared to experimental thermodynamic measurements leading to putative binding models. Thanks to this

interesting biological profile **20** can be considered a multitarget anticancer agent and a promising lead compound for this class of derivatives.

Introduction

Naphtalene diimide (NDI) scaffold is present in a wide number of potential anticancer agents which interact with DNA preferentially as intercalators[1-5]. Additionally, some derivatives characterized by this core have been optimized to exhibit bis-threading intercalating ability[6], to enhance the stabilization of DNA triplexes[7], to stabilize[8] or alkylate[9,10] G-quadruplex DNA structure.

One of the main prototype of NDI derivatives is represented by N-BDMPrNDI (Figure 1) which showed the ability to intercalate into steps containing at least one G:C base pair.[11] Recently, we published a paper in which we reported a new series of NDI derivatives as antiproliferative agents.[12] These compounds were characterized by NDI scaffold properly functionalized with two basic side chains which, in principle, should enhance both their solubility in aqueous media and interactions with

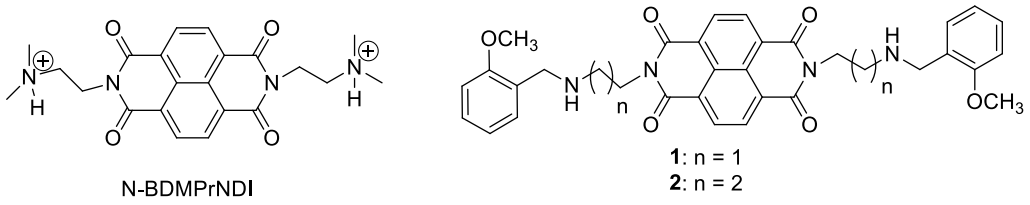

Figure 1. Chemical structures of N-BDMPrNDI, **1** and **2**.

the DNA phosphate groups.[13] This study was focussed on defining the influence of the length of the two basic side chains on antiproliferative activity by exploring linkers comprising from two to ten methylene units. A 2-methoxybenzyl substituent was introduced at the side chain terminal nitrogens because we reported its ability to

improve the basicity when inserted on terminal nitrogen atoms of polymethylene amines.[14] We identified two lead compounds **1** and **2** (Figure 1) which showed an interesting antiproliferative activity in the micromolar range on SKBR-3, CEM and HL60 cell lines. Furthermore, they efficiently interacted with DNA, they triggered caspase activation, caused p53 protein accumulation, down-regulated AKT survival, and finally, caused a decrease of ERK1/2 and inhibited ERKs phosphorylation. All these biological properties might indicate these derivatives as multitarget ligands[15]. Since, cancer is a complex disease comprising numerous altered biological networks, this new class of compounds might represent a more comprehensive treatment of pathology.[16]

In the present work we extended the study of structure-activity relationships of prototypes **1** and **2**, including the effect of different substituents on the phenyl rings. In particular, we introduced 2-methoxybenzyl groups in different positions of the two aromatic rings as well as other chemical groups characterized by different aromatic effects to verify a their possible influence on the biological activities. Since the two prototypes differ in the length of the two basic side chains, the new synthesized compounds were divided in two series, in particular the **1**-related series is constituted by the odd final derivatives **3**, **5**, **7**, **9**, **11**, **13**, **15**, **17**, **19**, and **21**; the **2**-related series by the even final compounds **4**, **6**, **8**, **10**, **12**, **14**, **16**, **18**, **20**, and **22**. To note that fluorine derivatives **11** and **12** were also investigated for the peculiar effects of this substituent in many different derivatives.[17]

Finally, the trimethoxybenzyl moiety, a common pharmacophore characterizing different well-known anticancer compounds such as Combrastatin A4, Colchicine and Podophyllotoxin all acting on tubulin skeleton, was inserted on the **1** and **2** scaffolds,

to give **19**-**22**, with the aim to include some other new targets in their anticancer activity.

All derivatives were screened by cytotoxic assays, and the more interesting were also evaluated by specific biological assays in order to elucidate their molecular mechanism. In particular, DNA interaction, apoptosis activation, specific enzymes inhibition investigations and molecular modelling studies were performed.

Results and discussion

Chemistry. Compounds **3-22** were synthesized following the procedure reported in Scheme 1 and were characterized by IR, ^{1}H NMR, mass spectra, and elemental analysis. The appropriate aldehydes were treated with 1,2-diaminoethane or 1,3-diaminopropane to afford the corresponding Schiff bases which were reduced with sodium borohydride to give compounds **23**-**42**. Condensation of such derivatives with naphthalenetetracarboxylic dianhydride led to the corresponding diamines-diimides **3**-**22**. Di-*p*-toluensulfonates salts of all the compounds were prepared to obtain derivatives easier to handle.

Scheme 1[a]

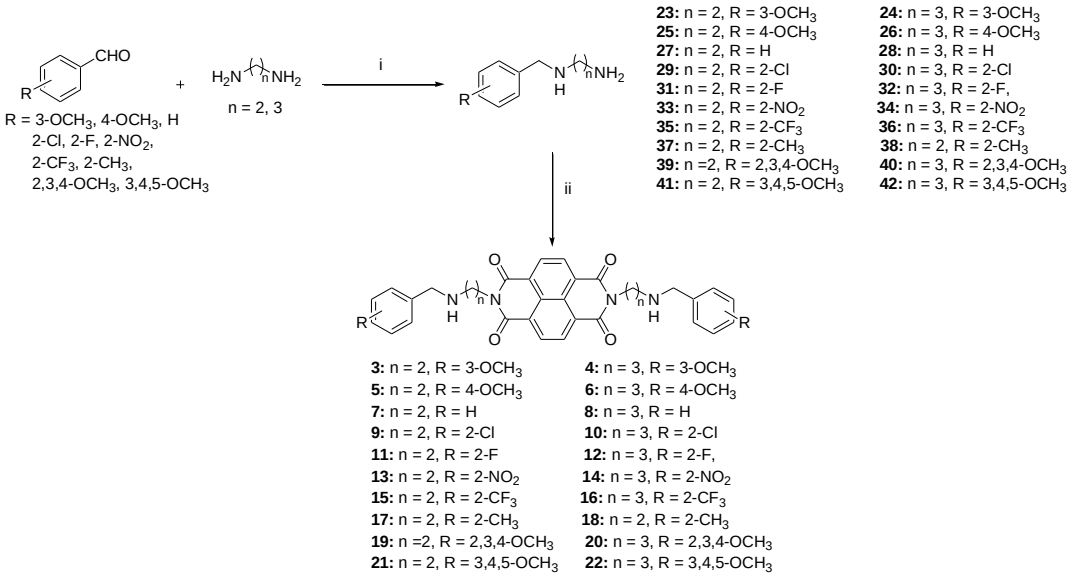

[a](i) (a) toluene, reflux, 3 h; (b) $NaBH_4$, EtOH, room temp., 3 h, 24-36%; (ii) 1,4,5,8-Naphthalene-tetracarboxylic dianhydride, i-PrOH, reflux, 12 h, 20-85%.

Biology

As preliminary screening all new compounds were submitted to the Developmental Therapeutics Program (DTP)[a] at National Cancer Institute (NCI) for evaluation of their anticancer activity against human cell lines. The most active compounds were been object of further investigations to better elucidate their molecular mechanism.

Growth-Inhibiting Activity. Although all substituted compounds of the two series were synthesized, only **8**, **10**, **12, 20** and **22** of the **2**-series together with **3**, **5, 19** and **21** of the **1**-series, in which the 2-methoxy group was moved at positions 3 and 4, respectively, were selected by National Cancer Institute (NCI, Bethesda), for evaluation in the full panel of about 60 human cancer cell lines. (Table 1). Finally, to complete the cytotoxic investigation of the **2**-series, the effects of compounds **14**, **16** and **18** on growth inhibition of a more limited panel of tumor cell lines including: HTLA-230, OVCAR-3, MZ2-Mel 3.0 and SW620 were investigated (Table 2).

Compounds **6**, **9**, **11**, **13**, **15**, **17** were evaluated only to a preliminary test at 10^{-5} μM concentration for 48 h incubation (data not shown). Indeed, only compounds that satisfied predetermined threshold inhibition criteria in a minimum number of cell lines, based on the analysis of historical Developmental Therapeutics Program (DTP) screening data, progressed to the full five-concentration assay. Following these criteria, derivatives **1**-**3**, **5**, **7**, **8**, **10**, **12**, **19**-**22** were selected for evaluation in the full panel of about 60 human cancer cell lines derived from nine human cancer cell types, that have been grouped in disease sub-panels including leukemia, non-small-cell lung, colon, central nervous system, melanoma, ovarian, renal, prostate, and breast tumor cell lines (Table 1). The compounds were dissolved in dimethyl sulfoxide and evaluated at five concentrations at 10-fold dilution the highest being 10^{-4}M and the others 10^{-5}, 10^{-6}, 10^{-7}, and 10^{-8}M[18-20] in comparison with our lead compounds **1** and **2**. Results showed in Table 1 are expressed as the negative log of the molar concentration at three assay end points: the 50% growth inhibitory power (pGI_{50}), the cytostatic effect (pTGI = total growth inhibition), and the cytotoxic effect (pLC_{50}). For several compounds this five concentration assay was repeated twice and no significative differences were found.

Regarding compounds related to **1**, we can observe that the removal of the methoxy group (**7**) or its shift to position 3, providing **3**, caused a decrease of cytotoxic activity of more than ten folds, as, while its introduction in position 4 (**5)**, restored completely the activity, which is comparable with that of the lead compound **1**. The introduction of additional two methoxy groups in position 3 and 4 (**19**) or in 4 and 5 (**21**), caused a decrease in the cytotoxic activity in comparison with **1**.

In the series of **2**-related compounds, we can observe that the substitution of the methoxy group with a hydrogen (**8**) or fluorine (**12**) atom, did not cause any decrease in activity. On the contrary the presence of different substituents such as chlorine (**10**), nitro (**14**), trifluoromethyl (**16**) and methyl (**18**) groups in 2 position on the two aromatic rings determined a marked decrease of inhibitory activity on different cell lines in comparison with **2**. In particular, it is to note that **16** did not show any significant activity up to 10 μM (Table 2). In this series the pattern of the multi-substitution with three methoxygroups is different from that observed for **1**-series. In fact compounds **20** and **22**, characterized by 2,3,4 and 3,4,5 trimethoxysubstitution, respectively, showed different activity. In particular, **22** showed a decrease in inhibition activity in comparison with **2**, on the contrary, **20** showed the highest levels of GI_{50} of the two series, emerging as the most potent derivative towards the different tested cell lines. Notably, this compound displayed the highest values of cytotoxic activity against the colon and prostate cells which are similar to those reported for vincristine, a well-known anticancer agent (see Table 1). These results indicated **20** as the most interesting derivative of the two series. Thus it was used as model compound for further investigations to elucidate its mechanism of action at cellular level.

Table 1. Growth Inhibition and Cytostatic and Cytotoxic Activity of **1**-**3**, **5**, **7**, **8**, **10**, **12**, **19**-**22** in the 60-Cell Panel

Compd[a]	modes	leukemia	NSCLC	colon	CNS	melanoma	ovarian	renal	prostate	breast	MG-MID[b]
1	pGI_{50}	6.60	6.44	6.7	6.29	6.34	6.53	6.34	6.52	6.34	6.46
	pTGI	6.17	6.07	6.35	5.89	5.95	6.05	5.92	6.02	5.88	6.03
	pLC_{50}	5.36	5.72	6.14	5.54	5.58	5.37	5.47	5.47	5.35	5.55
2	pGI_{50}	6.75	6.69	6.94	6.67	6.72	6.74	6.67	6.73	6.64	6.73
	pTGI	6.10	6.26	6.51	6.23	6.41	6.08	6.27	6.36	6.19	6.27
	pLC_{50}	6.01	5.74	6.03	5.80	6.09	5.42	5.73	5.82	5.79	5.82
3	pGI_{50}	5.57	5.24	5.66	5.50	5.72	5.72	5.46	5.41	5.58	5.54
	pTGI	5.05	4.98	5.30	5.04	5.42	5.42	5.04	4.76	5.13	5.13
	pLC_{50}		4.52	4.77	4.73	5.09	5.09	4.45	4.20	4.84	4.71
5	pGI_{50}	6.54	6.40	6.75	6.62	6.61	6.71	6.44	6.39	6.49	6.55
	pTGI	5.83	5.79	6.28	5.96	6.22	6.06	5.91	5.78	5.98	5.98
	pLC_{50}	4.72	5.17	5.75	5.44	5.83	5.40	5.48	5.38	5.36	5.39
7	pGI_{50}	5.90	5.64	5.90	5.63	5.79	5.62	5.60	5.57	5.72	5.71
	pTGI	5.30	5.20	5.57	5.04	5.44	5.24	5.21	4.94	5.24	5.24
	pLC_{50}		4.99	5.23	6.63	5.22	4.78	4.67		4.36	5.12
8	pGI_{50}	6.85	6.68	7.03	6.81	6.76	6.79	6.75	6.74	6.65	6.78
	pTGI	6.05	6.23	6.53	6.42	6.44	6.30	6.29	6.37	6.16	6.31
	pLC_{50}		5.71	5.90	5.95	6.12	5.36	5.67	5.69	5.57	5.74
10	pGI_{50}	6.58	6.48	6.86	6.35	6.73	6.65	6.63	6.38	6.48	6.57
	pTGI	5.79	5.96	6.37	5.86	6.13	6.15	6.15	5.88	6.03	6.03
	pLC_{50}	5.36	5.54	5.76	5.50	5.68	6.59	5.77	5.68	5.63	5.72
12	pGI_{50}	6.77	6.75	7.03	6.79	6.77	6.79	6.80	6,74	6.68	6.79
	pTGI	5.88	6.36	6.56	6.42	6.44	6.31	6.42	6.35	6.20	6.33
	pLC_{50}	4.70	6.03	6.14	5.96	6.17	5.87	5.82	6.26	5.93	5.87
19	pGI_{50}	6.42	6.32	6.77	6.20	6.52	6.67	6.50	6.19	6.45	6.45
	pTGI	5.93	5.85	6.33	5.74	6.09	6.49	6.26	5.91	5.94	6.06
	pLC_{50}		5.49	5.96	5.05	5.73	6.53	6.34		5.62	5.82
20	pGI_{50}	6.89	6.90	7.06	6.96	6.98	6.85	6.74	6.99	6.82	6.91
	pTGI	6.22	6.48	6.64	6.57	6.68	6.43	6.36	6.63	6.38	6.49
	pLC_{50}	4.66	5.91	6.10	6.07	6.39	5.64	5.90	6.13	5.96	5.86
21	pGI_{50}	6.65	6.28	6.60	6.41	6.28	6.39	6.36	6.71	6.58	6.47
	pTGI	6.29	5.92	6.02	5.94	6.01	6.04	6.09	6.13	6.20	6.07
	pLC_{50}		5.56	5.60	5.43	5.67	5.71	5.79	5.66	5.70	5.64
22	pGI_{50}	6.48	6.33	6.60	6.34	6.38	6.36	6.18	6.38	6.40	6.38
	pTGI	5.71	5.86	6.08	5.85	5.98	5.77	5.73	5.87	5.89	5.86
	pLC_{50}	5.38	5.70	5.41	5.37	5.58	5.26	5.27	5.33	5.31	5.40
vin[c]	pGI_{50}	7.00	6.60	7.00	6.90	6.80	6.50	6.50	6.90	6.50	6.74
	pTGI	4.80	4.80	5.40	5.20	5.10	4.70	4.70	5.20	5.10	5.00
	pLC_{50}	3.20	3.60	4.10	3.70	3.60	3.50	3.60	3.50	3.50	3.59

[a]**1**-**3**, **5**, **7**, **8**, **10**, **12**, **19**-**22**, di-*p*-toluensulfonate salts; highest concentration = 10^{-4}M unless otherwise reported; only modes showing a value greater than 4.00 are reported. [b]Mean graph midpoint, i.e., the mean concentration for all cell lines. [c]Vincristine sulfate, highest concentration = 10^{-3} M. Data are expressed as the negative log of the molar concentration at three assay end points: the 50% growth inhibitory power (pGI50), the cytostatic effect (pTGI = total growth inhibition) and the cytotoxic effect (pLC50).

Table 2. Cytotoxic Activity of **2**, **14**, **16**, and **18** against HTLA-230, OVCAR-3, Mel 3.0, and SV620 Cells

	pIC_{50}[b]				
compd[a]	HTLA	OVCAR	MZ2-Mel 3.0	SV620	MG/MID[d]
2	7.01 ± 0.31	6.70 ± 0.21	6.15 ± 0.07	6.40 ± 0.21	6.56
14	6.04 ± 0.17	6.15 ± 0.29	5.77 ± 0.05	6.22 ± 0.24	6.05
16	na[c]	na[c]	na[c]	na[c]	na[c]
18	6.04 ± 0.19	5.71 ± 0.35	5.72 ± 0.16	6.04 ± 0.05	5.88

[a]di-p-toluensulfonate salts. [b]IC_{50} values are the negative log of the molar concentration causing 50% growth inhibition, after 48 h of compounds exposure, evaluated by MTT method. [c]Not active at 10 μM. [d]Mean graph midpoint, i.e., the mean concentration for all cell lines. Results, derived from three different experiments in quadruplicate wells as compared to that of control cells, are expressed as mean ± S.E.M.

Effect of compound 20 on tumor cell proliferation. To give some insights into the biological effects of the novel compounds, the most potent derivative of the all series **20** was further investigated in HeLa cells. It largely reduced cell survival (Figure 2A) with a IC_{50} value of 0.85 μM. Firstly, we determined whether it induced apoptosis. HeLa cells were treated with **20** for 24 h, afterward the activity of caspase proteases was assayed. Activation of caspase acting on the substrate sequence Asp-Glu-Val-Asp (DEVD), i.e. mainly effector caspases -3 and -7, represents a marker of apoptotic cell death.[21] **20** increased caspase activity in a dose-dependent manner (Figure 2B), in association to the increased number of cells committed to death. We then evaluated nuclear morphology, which is another reliable indicator of apoptotic cell death, by DAPI staining in cells treated for 24 h with 2 μM of **20** (Figure 2C). In **20**-treated cells it was possible to detect several cells with characteristics of apoptosis, i.e. chromatin condensation, nuclear fragmentation and/or condensation.[22]

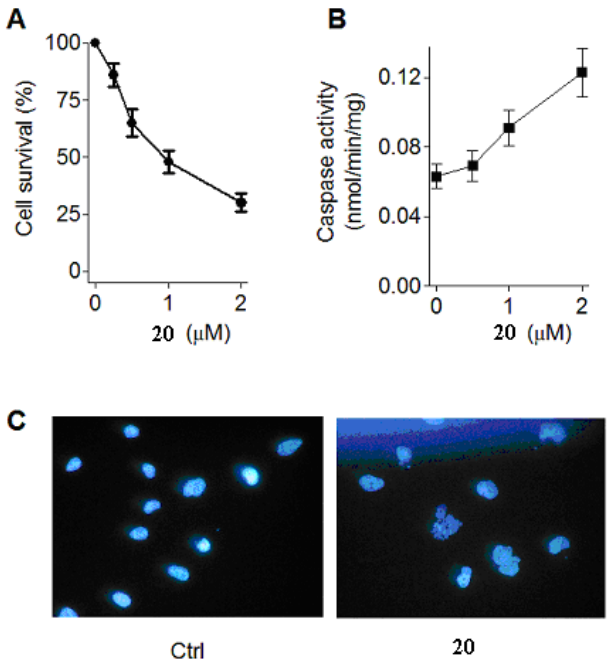

Figure 2. A. HeLa cells were incubated for 48 h in the presence of **20**, then the number of alive viable cells was measured by dye exclusion. **B.** The cells were treated for 24 h with the indicated dose of **20**, afterward, cells were collected for caspase activity determination. Data are mean ± S.E.M. of three replicates. **C**. Morphological evaluation of nuclei stained with DAPI from control HeLa cells and cells treated with 2 μM of **20** for 24 h.

Signal transduction pathway. We investigated the effect of **20** on signal transduction pathway involved in cell growth. In these studies, the cells were treated with **20** for 20 hours, then ERK1/2 mitogen-activated protein kinases that are generally associated with cell growth were examined. Figure 3 showed that **20** downregulated the p44 ERK2 protein, and significantly inhibited the phosphorylation of both p42 and p44 ERKs, which are known to influence the survival of cancer cells.[23]

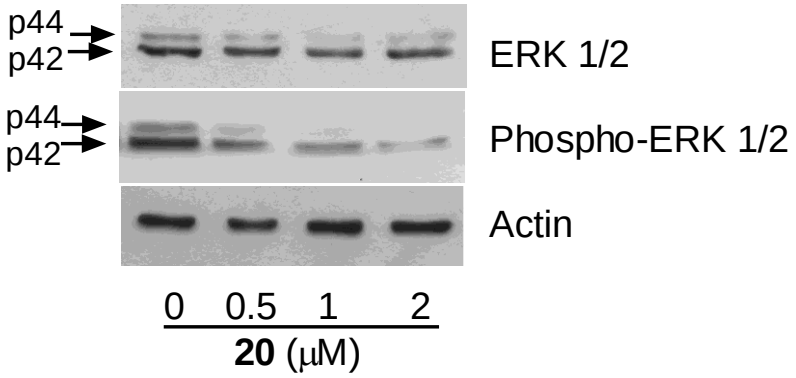

Figure 3. HeLa cells were incubated for 20 h in the presence of the indicated concentration of **20**. The content and phosphorylation status of ERK 1/2 in cell extracts was determined by Western blotting (50 μg of protein/lane).

In order to detect whether oxidative stress would play a role in the cytotoxic effects of the novel derivatives, we studied the effect of the antioxidant N-acetylcysteine (NAC). Figure 4 shows that NAC inhibited the toxic effect of **20**, suggesting the involvement of an oxidative mechanisms.

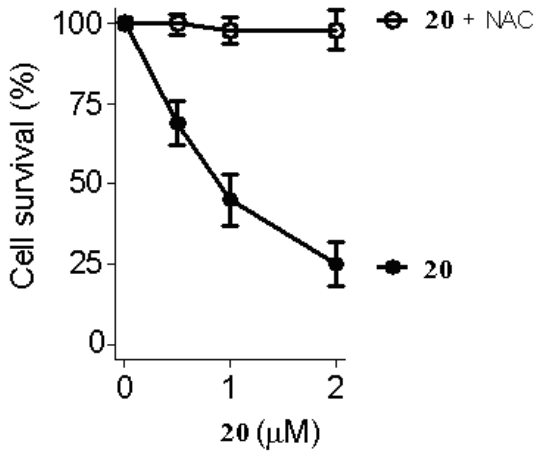

Figure 4. Cell viability was measured in cells treated for 24 h with the indicated concentration of **20** in the absence or presence of 5 mM NAC. Results are mean ± S.E.M. of triplicate determinations.

Effect of 20 on Cell Cycle Progression. To investigate whether the antiproliferative effect displayed by **20** was associated to a inhibition of cell cycle progression HTLA-230 neuroblastoma cells were treated with 1.5 µM of **20** for 24-48 hours. The cells were then pulsed labelled with BrdU to examine DNA synthesis. As shown in Fig. 5, we observed a time-dependent increase of the proportion of cells in G_2/M phases (R4) that was accompanied by a nearly complete depletion of cells in S phase (R3). In particular, the percentage of cells in S phase decreases from 33% to 9.6% while the percentage of cells accumulated in G_2/M phases was of 30% after 48 h of treatment. Moreover, the percentage of cells in the sub-G1 fraction (R1), which contains apoptotic cells, increased at longer times of **20** exposure (from 0.9% to 15.2% after 48 h). Therefore the cell cycle analysis showed a concomitant rise of treated cells in G_2/M fraction and a depletion of S fraction. These findings suggest delay in exit of daughter cells from the mitotic cycle leading to reduction of tumor cell number.

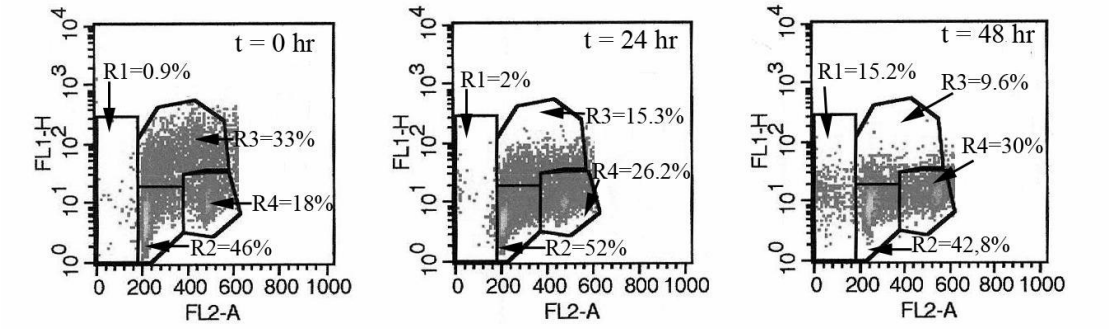

Figure 5. Effect of **20** on cell cycle progression in HTLA-230 neuroblastoma cells.

HTLA-230 were exposed to 1.5 μM of **20** for the indicated times and then the cells were analysed for DNA synthesis by pulse labelling with bromodeoxyuridine. BrdU uptake (fluorescein isothiocynate, *y*-axis) versus total cellular DNA content (propidium iodide, *x*-axis) was evaluated by densitometric fluorescence-activated cell sorter analysis.(R1 = sub-G_1-phase cells; R2 = G_1-phase cells; R3 = S-phase cells; R4 = G_2/M-phase cells).

Annexin V flow cytometric analysis of apoptosis. We evaluated the apoptosis in OVCAR 3.0 cells treated with **20** by staining cells with Annexin V-FITC and PI, FACS was used to distinguish and quantitatively determine the percentage of dead, viable, apoptotic and necrotic cells. As shown in Figure 6 panel A, OVCAR 3.0 control and treated cells were gated into LR (Lower Right), UP (Upper Right), LL (Lower Left) and UL (Upper Left) quadrants. Cells in LR and UR were considered as early apoptotic (annexin$^+$/PI$^-$) and late apoptotic (annexin$^+$/PI$^+$) respectively. Cells in LL and UL were considered live (annexin$^-$/PI$^-$) and necrotic (annexin$^+$/PI$^+$) respectively. We reported the most representative experiment after 72 h of drug exposure: the percentage of total apoptosis recorded in treated cells was 41% at 1.5 μM, 47% at 2.0 μM and 57% at 2.5 μM. These data confirmed the apoptotic mode of cell death. The experiment was repeated three times with similar results.

In Figure 6 panel B the extent of apoptosis was expressed as the sum of the percentages in LR and UR quadrants. Compound **20** was effective in inducing apoptosis in a dose and time dependent manner. The mean values and standard deviations calculated for untreated and treated cells at different concentrations in combination with the statistical analysis determined by Mann Whitney test

demonstrated that the differences between control and treated cells are statistically significative at any time of treatment (P = 0.0286 vs control).

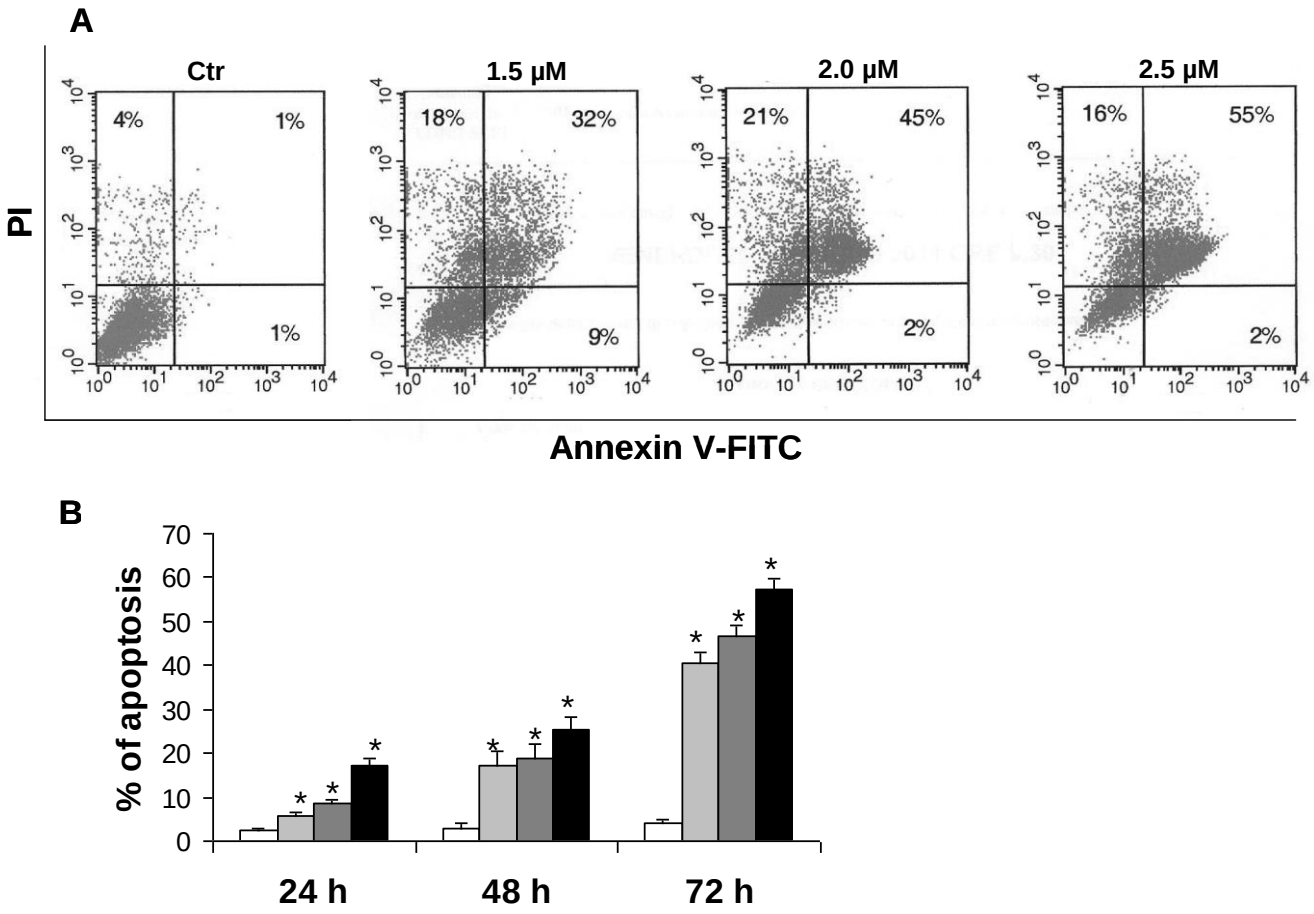

Figure 6. (A) Representative flow cytometry analysis of apoptosis induced by **20** at different concentrations in OVCAR 3.0 ovarian carcinoma cell line after 72 h of drug exposure, using annexin V-FITC/PI double staining method. Quadrant analysis of fluorescence intensity of gated cells in FL-1 (annexin V-FITC) and FL-3 (PI) channels was from 10,000 events. The lower left quadrant shows viable cells; the lower right quadrant shows viable cells in early stages of apoptosis; the upper right quadrant shows cells in the later stage of apoptosis; and the upper lower left quadrant shows dead cells. (B) Quantitative detection of **20**-induced apoptosis by Annexin V-FITC/PI staining on OVCAR 3.0 cell line at different times and concentrations. White

columns: control; light grey columns: **20** compound 1.5 μM; grey columns: **20** compound 2.0 μM; black columns: **20** compound 2.5 μM. Bars represent the mean number of triplicates wells from three independent experiments; statistical significance of differences between untreated and treated groups at different times was determined by Mann-Whitney test., two tailed, with 95% confidence intervals. * $P = 0.0286$ vs controls.

Tubuline Assays. As above reported, derivatives **19**-**22** were designed by introducing the trimethoxyphenyl pharmacophore, peculiar of some anticancer agents such as colchicine, podophyllotoxin and combrestatin A4 which affect the microtubules structure, with the aim to hit this specific and important biological target.

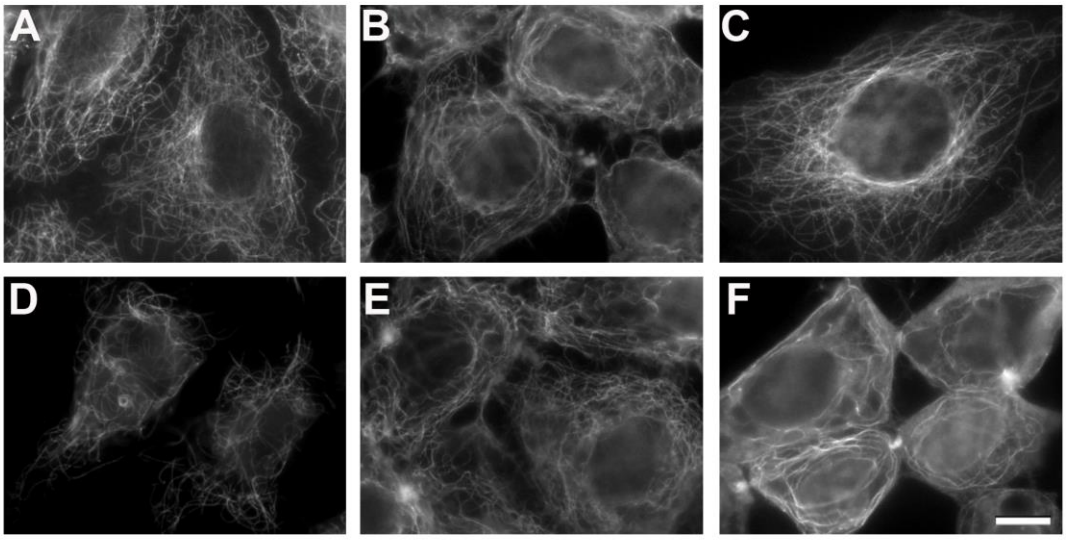

Figure 7. Effect of **19**-**22** and reference compound **2** on the cytoplasmic microtubule network of A549 lung carcinoma cells. A549 cells were incubated for 20 hours with either A, DMSO, B, 10 μM **20**, C, 50 μM **19**, D, 50 μM **21**, E, 20 μM **22**,or F, 20 μM

2. Microtubules were stained with anti-tubulin monoclonal antibodies (DM1A). The bar is 10 μm.

To verify this interesting biological activity **19**-**22** and the reference compound **2** were tested both in cells and *in vitro* assays. Concerning the first series of assays, A549 cells were incubated for 20 hours with 100 times the GI_{50} of **19**-**22** and **2**. In these experiments no depolimerization of the cytoplasmic microtubules was observed (Figure 7). In particular, when the cells were treated with **21** and **2** (Figure 7, D, F) the cells became rounded and the microtubule cytoskeleton looked disorganized but no microtubule depolimerization was observed. As control 2.5 μM podophilotoxin was employed and the cellular microtubules completely depolimerized (results not shown).

Concerning the *in vitro* assay we tested the assembly of 25 uM tubulin in the presence of 30 μM of **2**, **19**-**21**. In the absence of compounds the critical concentration of tubulin required for assembly was 3,40 ± 0.83 uM. In the presence of a stabilizer (docetaxel) the concentration was of course lower 1,24 ± 0.31 uM. In the presence of a destabiilizer (podofilotoxin) the concentration required is lower 7.40 ± 0.79 μM. In the presence of the compounds **2**, **19**-**21** the required concentration was equal to those required in the absence of drug 3.67 ± 0.90 3.65 ± 0.97 3.23 ± 0.86 3.50 ± 1.09, respectively, and no effect on tubulin assembly was observed.

These results demonstrated that **2**, **19**-**21** did not affect directly microtubules and tubulin. In particular, in A549 cells they were cytotoxic but they did not impair microtubules functions.

DNA-Binding properties. Several NDI derivatives are efficient DNA binders and this property can result in promotion of cell apoptosis. To preliminary assess the ability of the most interesting compounds of the **2** series (**8, 12, 20** and **22)** to interact with double stranded DNA, a fluorometric intercalator displacement method was applied.[24] DNA-binding activity was expressed as the drug concentration able to reducing by 50% the fluorescence of DNA-bound ethidium bromide (EtBr) Displacement. This EC_{50} value allows to estimate the affinity ranking order of the ligands for calf thymus DNA.[24, 25] All tested derivatives turned out to be strong DNA-interacting molecules (Table 3) with modest modulation of the EC_{50} values.

Table 3. DNA Binding of **1**, **2**, **8**, **12**, **20** and **22** evaluated by EtBr Displacement and fluorescence quenching determined at 2.5 μM ligands concentration.

	EtBr Displacement EC_{50} (nM)[a]	Fluorescence quencing ΔTm (°C)[b]	
Compound	ctDNA	G4	dsDNA
1	93 ± 4[c]	16.1	6.2
2	122 ± 6[c]	15.5	7.7
8	118 ± 8	18.5	11.3
12	130 ± 8	16.4	8.1
20	166 ± 8	20.5	8.4
22	159 ± 8	16.1	5.2

[a]EC_{50} values are defined as the drug concentrations which reduce the fluorescence of the DNA-bound ethidium by 50%. [b]ΔTm corresponds to the increment in the DNA melting temperature induced by 2.5 μM drug concentration. [c]Data reported in ref.12

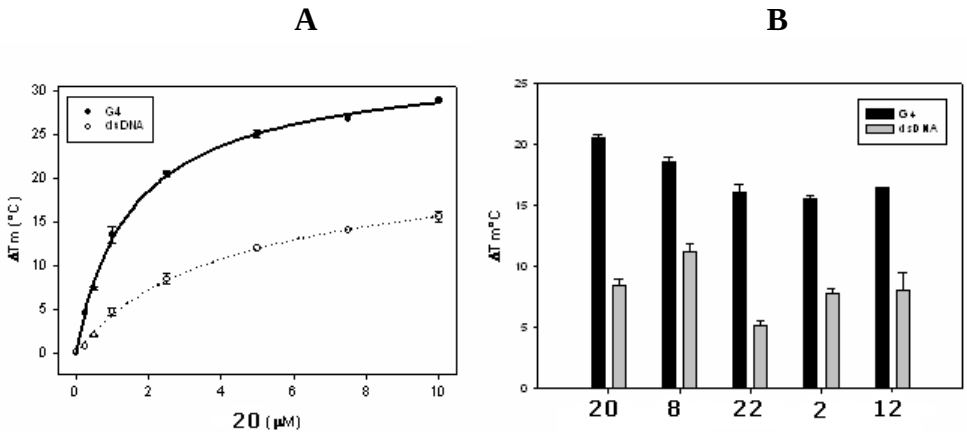

Figure 8. Variation of DNA (0.25 μM) thermal stability (ΔTm) produced by tested ligands in 50 mM potassium buffer, pH 7.4, evaluated by fluorescence quenching experiments. Heating rate 1 °C/min. PANEL A: increasing concentration of **20** on G-quadruplex DNA; PANEL B: **2**, **8**, **12**, **20**, and **22** (2.5 μM) on G-quadruplex (black bars) and dsDNA (grey bars).

Additionally, as reported in the literature, NDI derivatives can selectively interact with differently folded DNA structures accordingly to their substitution pattern and the nature of the side chains. Thus, the G-quadruplex and duplex DNA recognition of the selected NDI were compared by fluorescence quencing assay using a G-quadruplex folded sequence based on the human telomeric sequence (G4) and a random double stranded DNA (dsDNA). All derivatives were able to significantly increase the tested DNAs melting temperatures in a concentration dependent manner (Figure 8). It emerged that the increment in the melting temperature was generally more intense for the G-quadruplex folded sequence then for the dsDNA template. However, on both substrates, the process appeared to reach saturation in the low micromolar range, which suggests a strong interaction with both DNA arrangements. In Table 3 we report the shift in the DNA melting temperature induced by 2.5 μM

ligands concentration that confirmed modest efficiency variation among the tested compounds, in particular toward the G-quadruplex structure. However, **20** appears to be the most efficient G-quadruplex binder whereas **8,** in agreement with FID data, induced the most relevant stabilization on double stranded DNA. The difference between the recognition of the two DNA foldings slightly increments accordingly with the number of methoxy groups whereas, their substitution with a fluorine atom (**12**) does not significantly alter the DNA stabilization properties which parallels the cytotoxic effect.

The interaction of all derivatives with both substrates was further confirmed by CD spectroscopy. As reported in Figure 8, when NDI derivatives **2**, **8**, **12**, **20**, and **22** were added to a double stranded DNA an increment of the intensities of the two mayor bands located at 275 and 245 nm occurred. This confirms an intercalation binding mode for NDI into the double helix. When the substrate was the human telomeric G-quadruplex the binding of the ligand induced an increment of intensity of the 295 band which is generally attributed to the antiparralel components of the nucleic acid structure (Figure 9).

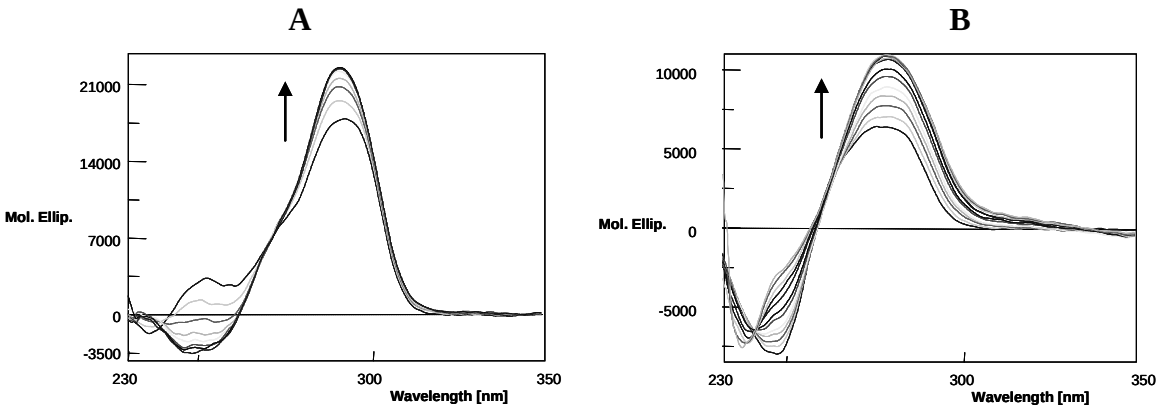

Figure 9. Modification of DNA CD spectra upon addition of **20** (0-20 μM) in 10 mM Tris, 50 mM KCl, pH 7.5. Arrows indicate spectrals changes upon ligand addition. Panel A: 4 μM Tel22, panel B, 45 μM ctDNA.

To get further insight into the NDI derivatives-DNA interaction, we performed a quantitative analysis of the binding process towards the two substrates using **20** as model compound. These data were obtained accoding UV-VIS titrations since addition of dsDNA or G-quadruplex DNA induced a significative reduction of the drug absorbance (Figure 10). The results of such an analysis are summarized in Table 4. These confirmed a relevant affinity of **20** toward both DNA substrates: the difference in Ka is likely not sufficient to preclude the recognition of one target in physiological conditions.

From these data we can additionally confirm that staking interactions are relevant for the DNA binding process. Indeed, dsDNA binding data analysis indicated a complex stoichimetry (n) of two base pairs for each bound drug molecule, which is in line with an intercalation binding mode. In the presence of G-quadruplex, we found two NDI molecules bound to one DNA structure. This likely corresponds to the staking of the ligands on each terminal tetrads.

Table 4. Thermodynamic parameters for the DNA binding by **20** determined in 10 mM Tris, 20 mM KCl, pH 7.5, 37°C. n refears to the number of G-quadruplex or base pairs involved in the binding of one NDI molecule.

	$Ka \cdot 10^{-6}$ (M^{-1})	n
G-quadruplex	6.94 ± 2.05	0.49 ± 0.01
dsDNA	0.85 ± 0.07	2.62 ± 0.03

Merging these results, we can infer that by incrementing the number of the methoxy groups on the side chains, the insertion of the aromatic portion (NDI core) between two base pairs of the double helix can be hindered. Indeed steric effect can occur to impair thereading of one side chain between two base pairs. On the opposite, this structural feature should not sensibly affect the staking mode of the NDI on the external G-quadruplex tetrads.

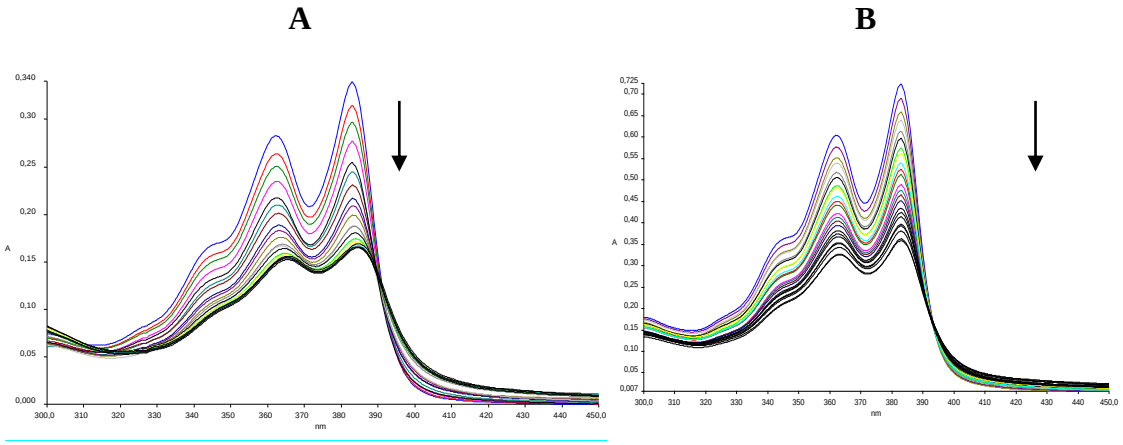

Figure 10. Titrations of **20** (10-20 μM) with DNA in 10 mM Tris, 50 mM KCl, pH 7.5. PANEL A: human telomeric sequence folded in G-quadruplex; PANEL B: ctDNA. Arrows indicate absorption spectra change upon DNA addition.

Taq Polymerase and Telomerase Inhibition Assays. Derivatives **1**, **2**, **8**, **12**, **20**, and **22** were evaluated for their inhibitory activity on Taq Polymerase. The most potent derivative was **22**, with **2** and **20** slightly less potent, but in the same order. Interestingly, **1** and **12**, characterized by shorter side chains and by a fluorine atom on

the aromatic rings, respectively, were the less potent of the all series, showing no activity up to 40 μM.

Since test derivatives showed to be able to recognize also telomeric G-quadruplex sequences, we additionally evaluated telomerase activity in HeLa cells treated with **20**, the best G-quadruplex binder. Our results confirmed that the tested NDI is able to reduce the activity of this enzyme thus confirming a cytotoxic mechanism which can result from the potential impairment of several biological pathways (Figure 11).

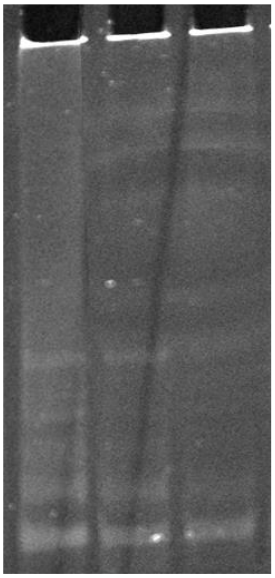

Figure 11. Reduction of telomerase activity in HeLa cell after treatment for 24 h with **20.** For each line, a cellular extract corresponding to 2 ng of total proteins was used.

Molecular modelling studies.

The most interesting compound **20** of the novel NDI series has been submitted to molecular modelling calculations with the aim to characterize its conformational

profile and to propose binding modes against the DNA target, accordingly to the experimental evidences.

Firstly, the ionization state of **20** has been analyzed with respect to the thermodynamic experimental conditions (pH = 7.5). Such an analysis was carried out by the program LigPrep.[26] The bis cationic form, with both secondary amines protonated, was indicated as the most prevalent among all ionisable states.

Secondly, in this ionization form, the conformational study has been carried out by the Monte Carlo search, as implemented in the MacroModel (version 9.0, 2009)[27] generating 10000 conformations and energy minimizing them by the AMBER* force field[28] with the united atom notation and the GB/SA water solvation model.[29] The number of conformers found within 5 kcal/mol above the global minimum was equal to 81.

Thirdly, the docking experiments were carried out selecting the DNA target models from the Protein Data Bank (PDB).[30] The selection of the DNA duplex model was performed by the analysis of intercalative ligands with resolution factor equal or lower than 1.5 Å. The PDB entry 1Z3F contains two guanine-citosine intercalative binding sites and the ligand (ellipticine) characterized by an extended aromatic core.[31] It was selected as template model for the DNA duplex docking.

As concerns the PDB G-quadruplex models, the availability of an NDI derivative co-crystal with the human telomeric sequence, led us to select as reference template model the 3CDM entry.[32]

Both duplex and G-quadruplex PDB entries were prepared for the docking eliminating non nucleic acid components, such as ligands, counterions and water molecules, included into the original models. As concerns the 3CDM entry, based on two DNA dimer subunits, both A and B chains were considered for the docking simulations.

The docking with the duplex DNA model was performed following the computational approach successfully tested with intercalative moieties in other antitumor compounds.[33] The target DNA was isolated in a conformation able to give intercalative recognition with ligands by stacking and groove interactions.

Accordingly to our last reported experiments we have considered two computational protocols based on Autodock[34] and Moline[35] docking programs. In both cases,

accordingly to the Moline general protocol[36] and to reported case studies,[37, 38] the best poses were submitted to full energy optimization in the same conditions used for the conformational search of the isolated compound **20**. The ensembles of optimized poses were then submitted to the estimation of free energy of complexation at room temperature.

The docking models obtained with Autodock were able to lead to energy minima lower than those with Moline. So we have analyzed them in details in order to characterize the recognition of **20** against the duplex and the quadruplex DNA conformations. The results of the Autodock optimized poses in terms of free energy of complexation are in agreement with the thermodynamic data reported in Table 4. Compound **20** docked with the DNA duplex model gave free energy of complexation equal to -92.2 kcal/mol, and with A and B G-quadruplex conformations values respectively equal to -66.2 and -79.3 kcal/mol. The reason of the high stability found with the DNA duplex can be understood analyzing the lowest energy pose reported in Figure 12, constructed by the LigandScout software.[39] There is a synergy of attractive interactions due to the NDI core stacking (two contributions) within the guanine-citosine intercalation site, one hydrophobic contact and hydrogen bond within the minor groove and two hydrogen bonds within the major groove. One of this last contributions is due to the *m*-methoxyl group of one side chain.

Conversely, the molecular recognition obtained in the docking simulations with the DNA G-quadruplex model was based in the best pose on few attractive contributions, as shown in Figure 13. Only one stacking interaction exerted by to one trimetoxyphenyl moiety was detected with the 8th nucleic residue (adenosine) located in a loop region of the target DNA G-quadruplex. The ligand established one hydrogen bond only with the 21st nucleotide (guanosine). The NDI core was not able to establish a proper end-stacking interaction with the G-quarter core in “top” or “bottom” sites, as classified in our previous communication.[40] The presence of the bulky trimethoxy sidechains likely prevented a good fit of the NDI core, as it happens with the ligand co-crystallized in the reference 3CMD PDB model. Moreover, the structure of **20** in the best pose highlights a certain difficulty to assume, into the binding region of the DNA G-quadruplex, an extended conformation, that can be

considered as a qualitative indicator of the steric hindrance in the recognition against this target.

In conclusion the docking experiments proposed different binding modes of interaction of **20** against duplex and G-quadruplex DNA models. The reason of a better recognition against the first target was justified in terms of superior non-covalent contributions and better fit properties of the ligand. The NDI core was able to establish stacking interactions *via* intercalative recognition with the duplex DNA only. The steric hindrance of the trimethoxy benzylamino propyl sidechains prevented a good NDI core end-stacking with the DNA G-quadruplex.

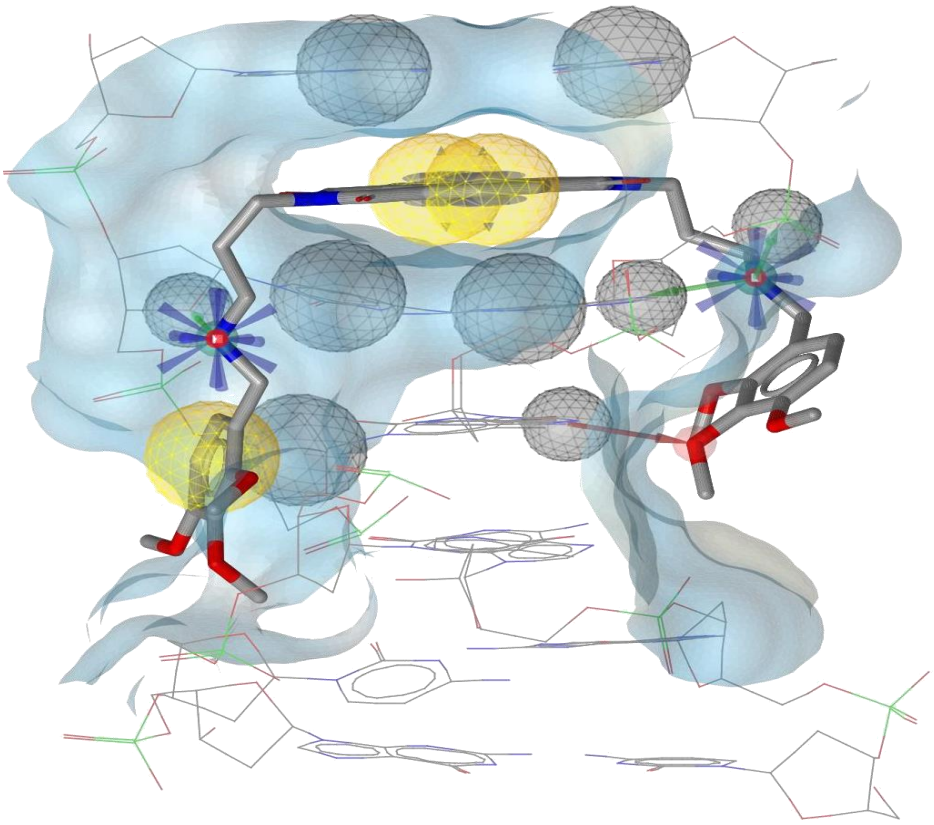

a)

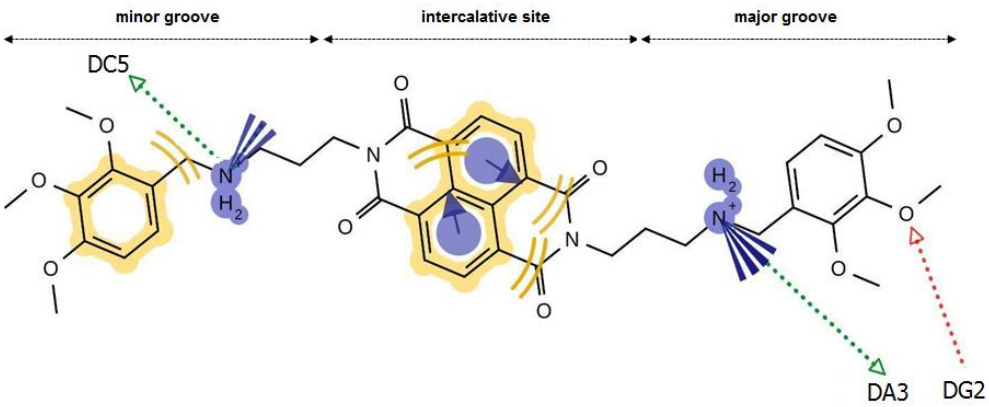

b)

Figure 12. a) 3D representation of the compound **20** best intercalative pose within the DNA duplex. The ligand and the DNA are respectively displayed as polytube and wireframe models. The gray surface represents target binding pocket. The hydrophobic features of the ligand are pointed as yellow spheres. The exclusion volume coats onto the target are shown as gray spheres. Intermolecular hydrogen bonds are displayed as red and green arrows, pointing respectively ligand acceptor and donor atoms. Positive ionizable target nitrogens are shown as blue features. The

ligand aromatic rings detected to interact *via* π-π interactions are highlighted with blue circles with top/bottom triangles.

b) 2D ligand representation with the main interaction features with the DNA duplex model. Three intermolecular hydrogen bonds are represented by dotted vectors. Electrostatic interacting nitrogens are shown as blue features. Hydrophobic interacting rings are highlighted in yellow. NDI core π-π stacked rings are depicted with blue circles and black arrows. The top ruler indicates the corresponding DNA duplex interaction area.

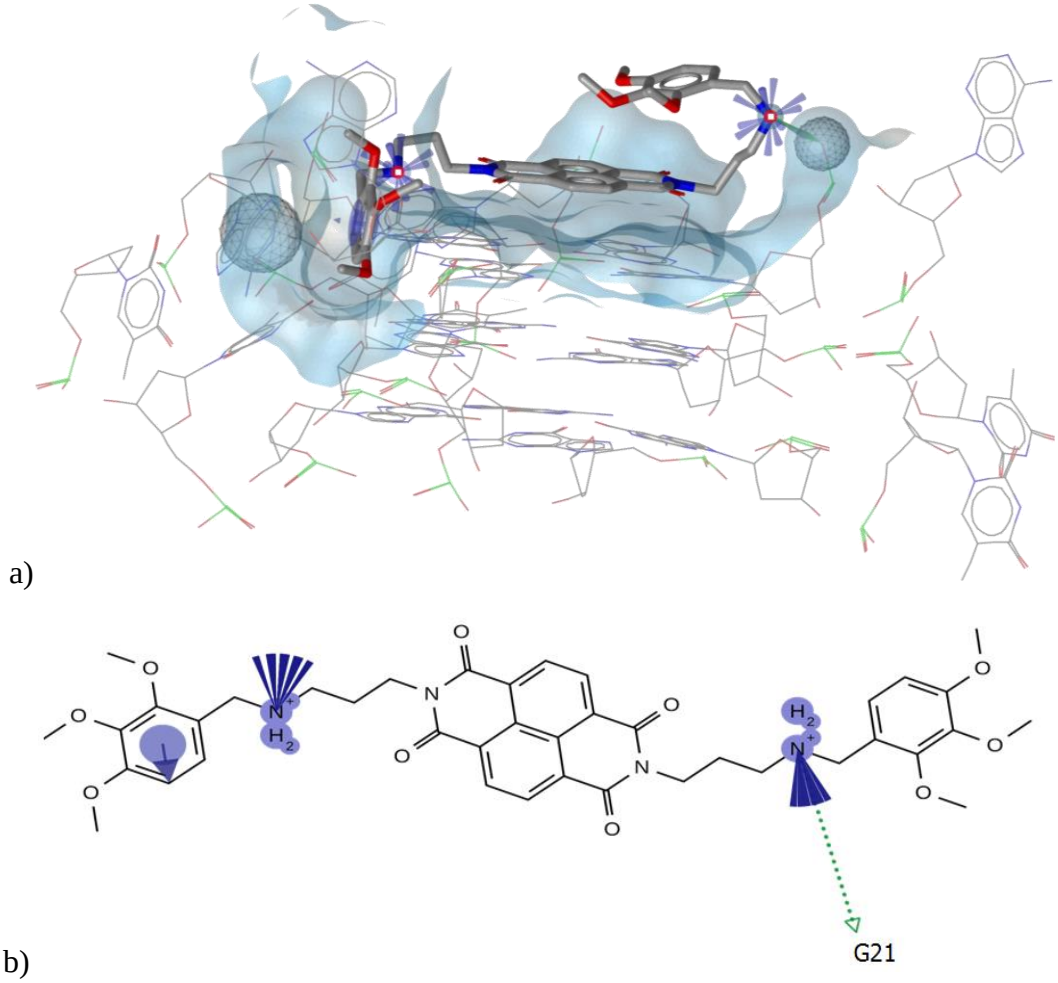

Figure 13. a) 3D representation of compound **20** best pose obtained with the DNA G-quadruplex model (PDB entry 3CDM chain B). The ligand and the DNA are respectively displayed as polytube and wireframe models. The gray surface represents target binding pocket. The exclusion volume coats onto the target are shown as gray spheres. The intermolecular donating hydrogen bond is displayed as green arrow.

Positive ionizable target nitrogens are shown as blue features. The ligand aromatic ring detected to interact *via* π-π interactions is highlighted with a blue circles with top/bottom triangles.
b) 2D ligand representation with the main interaction features with the DNA G-quadruplex model. One intermolecular hydrogen bond is represented by a dotted vector. Electrostatic interacting nitrogens are shown as blue features. The π-π stacked ring is depicted with blue circles and a black arrow.

Conclusion

The present article expands on the study of the structure-activity relationships of the prototypes **1** and **2**, especially by investigating the role of the substituents on the two aromatic rings included in the side chains. The cytostatic and cytotoxic activities of **1** and **2** were affected by the insertion of different substituents on the two aromatic rings confirming a their possible influence on the biological effects. Derivative **20**, characterized by a chain length of three methylene units and by 2,3,4-trimethoxy groups on the two aromatic rings, was the most potent of the all series showing an interesting biological profile. In fact, it displayed pGI_{50} values around 7, demonstrating an improvement of the cytotoxic activity towards multiple cancer lines, in comparison with lead compounds **1** and **2** and comparable with those of vincristine. Nevertheless, the mechanism of action of **20** is distinct from vincristine. Indeed, **20** showed the ability to tightly bind DNA, to inhibit Taq polymerase and telomerase, to trigger caspase activation by a possible oxidative mechanism, to downregulate ERK 2 protein and to inhibit ERKs phosphorylation, without acting directly on microtubules and tubuline.

According to these promising results, this compound might be considered a multitarget anticancer agent and a promising starting point for designing new antiproliferative agents.

(A) Chemistry. All the synthesized compound have a purity of at least 95% determined by HPLC analysis. Melting point were taken in glass capillary tubes on a Buchi SMP-20 apparatus and are uncorrected. ESI-MS spectra were recorded on Perkin-Elmer 297 and WatersZQ 4000. ^{1}H NMR and ^{13}C NMR were recorded on Varian VRX 200 and 400 instruments. Chemical shift are reported in parts per millions (ppm) relative to peak of tetramethylsilane (TMS) and spin multiplicities are given as s (singlet), brs (broad singlet), d (doublet), t (triplet), q (quartet) or m (multiplet) Although IR spectral data are not included (because of the lack of unusual features), they were obtained for all compounds reported, and they were consistent with the assigned structures. The elemental analysis was performed with Perkin Elmer elemental analyzer 2400 CHN. From all new compounds satisfactory elemental analyses were obtained, confirming >95%purity. Chromatographic separations were performed on silica gel columns by flash (Kieselgel 40, 0.040-0.063 mm, Merck) column chromatography. Reactions were followed by thin layer chromatography (TLC) on Merck (0.25 mm) glass-packed precoated silica gel plates (60 F254) and then visualized in an iodine chamber or with a UV lamp. The term “dried” refers to the use of anhydrous sodium sulphate.

General Procedure for the Synthesis of 3-22: a mixture of the appropriate amine **23-42** and 1,4,5,8-Naphthalene-tetracarbocylic dianhydride in a 1:5 molar ratio in *iso*-propanol were refluxed for 2 hours. After cooling down, removal of the solvent gave residue that was purified by flash chromatography using as eluent a mixture of dichloromethane/methanol/acqueous 33% ammonia (9:1:0.03) providing the desired products **3-22** that were converted into the corresponding di-*p*-toluenesulfonates salt.

2,7-Bis-[2-(3-methoxy-benzylamino)-ethyl]-benzo[lmn][3,8]phenanthroline-1,3,6,8-tetraone (3): yellow oil; 28% yield; ^{1}H NMR (free base, 200 MHz, $CDCl_3$) δ 1.58 (brs, 2H exchangeable with D_2O), 3.06 (t, 4H, J = 6.2), 3.76 (s, 6H), 3.84 (s, 4H), 4.41 (t, 4 H, J = 6.2), 6.85-6.89 (m, 4H), 7.18-7.29 (m, 4H), 8.78 (s, 4H); mp (di-paratoluensulfonates salt) 152-155°C, MS (ESI^+) m/z = 593 $(M+H)^+$. Anal. ($C_{48}H_{48}N_4O_{12}S_2 \cdot 2H_2O$), C, H, N.

2,7-Bis-[3-(3-methoxy-benzylamino)-propyl]-benzo[lmn][3,8]phenanthroline-1,3,6,8-tetraone (4): yellow oil; 16% yield; ^{1}H NMR (free base, 200 MHz, $CDCl_3$) δ 1.99-2.10 (m, 4H + 2H exchangeable with D_2O), 2,77 (t, 4H, J = 6.6), 3.81 (s, 10H), 4.34 (t, 4H, J = 7.7), 6.75-6.80 (m, 2H), 6.88-6.92 (m, 4H), 7.17-7.25 (m, 2H), 8.76 (s, 4H); ^{13}C NMR (50MHz, $CDCl_3$) δ 28.2, 39.0, 46.5, 53.8, 55.3, 112.4, 113.7, 120.5, 126.6, 128.0, 129.4, 131.1, 158.7, 163.8; mp (di-paratoluensulfonates salt) 102-104°C; MS (ESI^+) m/z = 621 $(M+H)^+$. Anal. ($C_{50}H_{52}N_4O_{12}S_2 \cdot 2H_2O$), C, H, N.

2,7-Bis-[2-(4-methoxy-benzylamino)-ethyl]-benzo[lmn][3,8]phenanthroline-1,3,6,8-tetraone (5): yellow oil, 15.0 % yield; ^{1}H NMR (free base, 400 MHz, $CDCl_3$) δ 1.54 (brs, 2H exchangeable with D_2O), 3.02 (t, 4H, J = 6.4), 3.74 (s, 6H); 3.76 (s, 4H); 4.37 (t, 4H, J = 6.4); 6.74-6.76 (m, 4H); 7.16-7.18 (m, 4H); 8.75 (s, 4H), mp (di-paratoluensulfonates salt) 124-126°C; MS (ESI^+) m/z = 593 $(M+H)^+$. Anal. ($C_{48}H_{48}N_4O_{12}S_2 \cdot 2H_2O$), C, H, N.

2,7-Bis-[3-(4-methoxy-benzylamino)-propyl]-benzo[lmn][3,8]phenanthroline-1,3,6,8-tetraone (6): yellow oil; 21% yield; ^{1}H NMR (free base, 200 MHz, $CDCl_3$) δ 1.59 (brs, 2H exchangeable with D_2O), 2.00 (m, 4H), 2.75 (t, 4H, J = 6.4), 3.75 (s, 4H), 3.79 (s, 6H), 4.32 (t, 4H, J = 7.0), 6.80-6.84 (m, 4H), 7.20-7.28 (m, 4H), 8.77 (s,

4H); mp (di-paratoluensulfonates salt) 134-136°C; MS (ESI^+) *m*/*z* = 621 $(M+H)^+$. Anal. ($C_{50}H_{52}N_4O_{12}S_2 \cdot 2H_2O$), C, H, N.

2,7-Bis-(2-benzylamino-ethyl)-benzo[lmn][3,8]phenanthroline-1,3,6,8-tetraone (7): yellow oil; 30% yield; ^1H NMR (free base, 200 MHz, $CDCl_3$) δ 1.58 (brs, 2H exchangeable with D_2O); 3.07 (t, 4H, *J* = 6.2), 3.88 (s, 4H), 4.42 (t, 4H, *J* = 6.6), 7.23-7.29 (m, 10H), 8.79 (s, 4H); ^{13}C NMR (50 MHz, $CDCl_3$) δ 40.6, 46.9, 53.6, 126.7, 127.0, 128.2, 128.5, 131.1, 151.1, 152.0, 163.2; mp (di-paratoluensulfonates salt) 163-165°C; MS (ESI^+) *m*/*z* = 533 $(M+H)^+$. Anal. ($C_{46}H_{44}N_4O_{10}S_2 \cdot 2H_2O$), C, H, N.

2,7-Bis-(3-benzylamino-propyl)-benzo[lmn][3,8]phenanthroline-1,3,6,8-tetraone (8): yellow oil; 34% yield; ^1H NMR (free base, 200 MHz, $CDCl_3$) δ1.45-1.45 (m, 2H + 4H exchangeable with D_2O), 3.15 (t, 4H, *J* = 6.2), 3.76 (s, 4H), 4.32 (t, 4H, *J* = 6.6), 7.17-7.25 (m, 10H), 8.72 (s, 4H); mp (di-paratoluensulfonates salt) 163-165°C; MS (ESI^+) *m*/*z* = 561 $(M+H)^+$. Anal. ($C_{48}H_{48}N_4O_{10}S_2 \cdot 2H_2O$), C, H, N.

2,7-Bis-[2-(2-chloro-benzylamino)-ethyl]-benzo[lmn][3,8]phenanthroline-1,3,6,8-tetraone (9): yellow oil; 35% yield; ^1H NMR (free base, 200 MHz, $CDCl_3$) δ 1.61 (brs, 2H exchangeable with D_2O), 3.06 (t, 4H, *J* = 6.6), 3.97 (s, 4H), 4.42 (t, 4H, *J* = 6.6), 7.17-7.19 (m, 4H), 7.28-7.35 (m, 4H), 8.78 (s, 4H); mp (di-paratoluensulfonates salt) 174°C; MS (ESI^+) *m*/*z* = 601 $(M+H)^+$. Anal. ($C_{46}H_{42}Cl_2N_4O_{10}S_2 \cdot 2H_2O$), C, H, N.

2,7-Bis-[3-(2-chloro-benzylamino)-propyl]-benzo[lmn][3,8]phenanthroline-1,3,6,8-tetraone (10): yellow oil; 21% yield; ^1H NMR (free base, 200 MHz, $CDCl_3$) δ 1.69 (brs, 2H exchangeable with D_2O), 1.95-2.08 (m, 4H), 2.78 (t, 4H, *J* = 7.0), 3.90 (s, 4H), 4.34 (t, 4H, *J* = 7.0), 7.16-7.24 (m, 4H), 7.28-7.40 (m, 4H), 8.76 (s, 4H); ^{13}C NMR (50 MHz, $CDCl_3$) δ 28.4, 39.1, 46.6, 51.2, 126.7, 126.8, 128.3, 129.5, 130.1,

131.0, 133.8, 137.7, 151.2, 163.0; mp (di-paratoluensulfonates salt) 115°C; MS (ESI^+) m/z = 629 $(M+H)^+$. Anal. ($C_{48}H_{44}Cl_2N_4O_{10}S_2 \cdot 2H_2O$), C, H, N.

2,7-Bis-[2-(2-fluoro-benzylamino)-ethyl]-benzo[lmn][3,8]phenanthroline-1,3,6,8-tetraone (11): yellow oil; 27% yield; ^1H NMR (free base, 200 MHz, $CDCl_3$) δ 1.62 (brs, 2H exchangeable with D_2O), 3.06 (t, 4H, J = 6.2), 3.85 (s, 4H), 4.41 (t, 4H, J = 6.2), 6.95-7.05 (m, 8H), 8.78 (s, 4H); mp (di-paratoluensulfonates salt) 174°C dec; MS (ESI^+) m/z = 569 $(M+H)^+$. Anal. ($C_{46}H_{44}F_2N_4O_{10}S_2 \cdot 2H_2O$), C, H, N.

2,7-Bis-[3-(2-fluoro-benzylamino)-propyl]-benzo[lmn][3,8]phenanthroline-1,3,6,8-tetraone (12): yellow oil; 22% yield; ^1H NMR (free base, 200 MHz, $CDCl_3$) δ 1.73 (brs, 2H exchangeable with D_2O), 1.90-2.08 (m, 4H), 2.77 (t, 4H, J = 7.0), 3.87 (s, 4H), 4.33 (t, 4H, J = 7.4), 6.97-7.21 (m, 4H), 7.23-7.37 (m, 4H), 8.76 (s, 4H); ^{13}C NMR (50 MHz, $CDCl_3$) δ 28.3, 39.0, 46.5, 47.3, 115.5, 124.1, 126.7, 128.6, 128.8, 130.4, 130.5, 131.01, 151.1, 163.0; mp (di-paratoluensulfonates salt) 104-107°C; MS (ESI^+) m/z = 597 $(M+H)^+$. Anal. ($C_{48}H_{46}F_2N_4O_{10}S_2 \cdot 2H_2O$), C, H, N.

2,7-Bis-[2-(2-nitro-benzylamino)-ethyl]-benzo[lmn][3,8]phenanthroline-1,3,6,8-tetraone (13): yellow oil; 26% yield; ^1H NMR (free base, 200 MHz, $CDCl_3$) δ 1.62 (brs, 2H exchangeable with D_2O), 3.08 (t, 4H, J = 6.2), 4.11 (s, 4H), 4.41 (t, 4H, J = 6.2), 7.28-7.54 (m, 6H), 7.80-7.85 (m, 2H), 8.78 (s, 4H); ^{13}C NMR (50 MHz, $CDCl_3$) δ 40.3, 47.1, 50.6, 124.7, 126.7, 128.1, 131.0, 131.3, 133.0, 135.4, 149.3, 151.3, 163.2; mp (di-paratoluensulfonates salt) > 250°C; MS (ESI^+) m/z = 623 $(M+H)^+$. Anal. ($C_{46}H_{42}N_6O_{14}S_2 \cdot 2H_2O$), C, H, N.

2,7-Bis-[3-(2-nitro-benzylamino)-propyl]-benzo[lmn][3,8]phenanthroline-1,3,6,8-tetraone (14): yellow oil; 24% yield; ^1H NMR (free base, 200 MHz, $CDCl_3$) δ 1.83 (brs, 2H exchangeable with D_2O), 1.85-1.97 (M, 4H), 2.77 (t, 4H, J = 6.6), 4.06 (s,

4H), 4.32 (t, 4H, *J* = 7.0), 7.36-7.44 (m, 2H), 7.53-7.66 (m, 4H), 7.92-7.96 (m, 2H), 8.74 (s, 4H); ^{13}C NMR (50 MHz, $CDCl_3$) δ 28.4, 39.0, 46.9, 50.8, 124.8, 126.6, 128.0, 131.1, 131.3, 133.2, 135.7, 149.2, 163.0; mp (di-paratoluensulfonates salt) 90-95°C; MS (ESI^+) *m*/*z* = 651 $(M+H)^+$. Anal. ($C_{48}H_{46}N_6O_{14}S_2 \cdot 2H_2O$), C, H, N.

2,7-Bis-[2-(2-trifluoromethyl-benzylamino)-ethyl]-benzo[lmn][3,8]phenanthroline-1,3,6,8-tetraone (15): yellow oil; 25% yield; ^{1}H NMR (free base, 200 MHz, $CDCl_3$) δ 1.59 (brs, 2H exchangeable with D_2O), 3.08 (t, 4H, *J* = 6.2), 4.03 (s, 4H), 4.43 (t, 4H, *J* = 6.2), 7.21-7.63 (m, 8H), 8.79 (s, 4H); ^{13}C NMR (50 MHz, $CDCl_3$) δ 40.4, 47.1, 49.6, 103.2, 125.9, 126.0, 126.7, 127.0, 128.3, 130.2, 131.1, 131.9, 138.8, 163.1; mp (di-paratoluensulfonates salt) 122-126°C; MS (ESI^+) *m*/*z* = 669 $(M+H)^+$. Anal. ($C_{48}H_{42}F_6N_4O_{14}S_2 \cdot 2H_2O$), C, H, N

2,7-Bis-[3-(2-trifluoromethyl-benzylamino)-propyl]-benzo[lmn][3,8]phenanthroline-1,3,6,8-tetraone (16): yellow oil; 27% yield; ^{1}H NMR (free base, 200 MHz, $CDCl_3$) δ 1.58 (brs, 2H exchangeable with D_2O), 2.02 (m, 4H), 2.81 (t, 4H, *J* = 7.0), 3.98 (s, 4H), 4.35 (t, 4H, *J* = 6.2), 7.29-7.38 (m, 2H), 7.47-7.55 (m, 2H), 7.62-7.65 (m, 4H), 8.78 (s, 4H); mp (di-paratoluensulfonates salt) 119-121°C; MS (ESI^+) *m*/*z* = 697 $(M+H)^+$. Anal. ($C_{50}H_{46}F_6N_4O_{14}S_2 \cdot 2H_2O$), C, H, N

2,7-Bis-[2-(2-methyl-benzylamino)-ethyl]-benzo[lmn][3,8]phenanthroline-1,3,6,8-tetraone (17): yellow oil; 28% yield; ^{1}H NMR (free base, 200 MHz, $CDCl_3$) δ 1.53 (brs, 2H xchangeable with D_2O), 2.27 (s, 6H), 3.08 (t, 4H, *J* = 6.4), 3.82 (s, 4H), 4.39 (t, 4H, *J* = 6.4), 7.05-7.08 (m, 5H), 7.21-7.26 (m, 3H), 8.74 (s, 4H); ^{13}C NMR (50MHz, $CDCl_3$) δ 19.2, 40.7, 47.3, 51.5, 126.0, 126.8, 1267.0, 127.1, 128.6, 130.4, 131.2, 136.5, 138.3, 163.3; mp (di-paratoluensulfonates salt) 149-151°C; MS (ESI^+) *m*/*z* = 561 $(M+H)^+$. Anal. ($C_{48}H_{48}N_4O_{10}S_2 \cdot 2H_2O$), C, H, N

2,7-Bis-[3-(2-methyl-benzylamino)-propyl]-benzo[lmn][3,8]phenanthroline-1,3,6,8-tetraone (18): yellow oil; 37% yield; ^{1}H NMR (free base, 200 MHz, $CDCl_3$) δ 1.64 (brs, 2H exchangeable with D_2O), 2.03 (m, 4H), 2.37 (s, 6H), 2.83 (t, 4H, *J* = 7.0), 3.80 (s, 4 H), 4.34 (t, 4H, *J* = 7.0), 7.14-7.15 (m, 5H), 7.25-7.28 (m, 3H), 8.76 (s, 4H); ^{13}C NMR (50 MHz, $CDCl_3$) δ 18.9, 28.2, 39.0, 46.9, 51.4, 125.7, 126.4, 126.5, 126.8, 128.2, 130.1, 130.8, 136.2, 138.1, 162.8; mp (di-paratoluensulfonates salt) 137-140°C; MS (ESI$^+$) *m*/*z* = 589 (M +H)$^+$. Anal.($C_{50}H_{52}N_4O_{10}S_2 \cdot 2H_2O$), C, H, N

2,7-Bis-[2-(2,3,4-trimethoxy-benzylamino)-ethyl]-benzo[lmn][3,8]phenanthroline-1,3,6,8-tetraone (19): yellow oil; 27% yield; ^{1}H NMR (free base, 400 MHz, $CDCl_3$) δ 1.90 (brs, 2H exchangeable with D_2O), 3.01 (t, 4H, *J* = 12.8), 3.49-3.90 (m, 22H), 4.38 (t, 4H, *J* = 8.7), 6.56-6.58 (d, 2H, *J* = 8.4), 6.92-6.94 (d, 2H, *J* = 8.4), 8.75 (s, 4H); ^{13}C NMR (100 MHz, $CDCl_3$) δ 40.1, 46.4, 48.4, 50.2, 55.8, 60.6, 106.8, 124.1, 125.2, 126.5, 126.6, 130.7, 141.9, 151.9, 153.0, 163.2; mp (di-paratoluensulfonates salt) 237°C dec; MS (ESI$^+$) *m*/*z* = 735 (M +Na)$^+$. Anal.($C_{52}H_{56}N_4O_{16}S_2 \cdot 2H_2O$), C, H, N

2,7-Bis-[3-(2,3,4-trimethoxy-benzylamino)-propyl]-benzo[lmn][3,8]phenanthroline-1,3,6,8-tetraone (20): yellow oil; 46% yield; ^{1}H NMR (free base, 400 MHz, $CDCl_3$) δ 1.96-2.0 (m, 4H + 2H exchangeable with D_2O), 2.74 (t, 4H, *J* = 8.0), 3.73 (s, 4H), 3.82 (s, 6H), 3.84 (s, 6H), 3.90 (s, 6H), 4.29 (t, 4H, *J* = 8.0), 6.56-6.58 (d, 2H, *J* = 8.0), 6.92-6.94 (d, 2H, *J* = 8.0), 8.73 (s, 4H); ^{13}C NMR (100 MHz, $CDCl_3$) δ 28.1, 38.9, 46.4, 48.4, 55.8, 60.6, 60.9, 106.8, 123.9, 125.7, 126.3, 126.4, 130.7, 141.9, 151.9, 152.8, 162.6; mp (di-paratoluensulfonates salt) 237°C dec; MS (ESI$^+$) *m*/*z* = 741 (M +H)$^+$. Anal.($C_{54}H_{60}N_4O_{16}S_2 \cdot 2H_2O$), C, H, N

2,7-Bis-[2-(3,4,5-trimethoxy-benzylamino)-ethyl]-benzo[lmn][3,8]phenanthroline -1,3,6,8-tetraone (21): yellow oil; 39% yield; ^{1}H NMR (free base, 200 MHz, $CDCl_3$) δ 1.52 (brs, 2H exchangeable with D_2O), 3.04 (t, 4H, J = 6.4), 3.74-3.80 (m, 22H), 4.38 (t, 4H, J = 6.3), 6.52 (s, 4H), 8.74 (s, 4H); ^{13}C NMR (50 MHz, $CDCl_3$) δ 40.2, 46.7, 53.6, 55.9, 60.7, 104.7, 126.5, 126.6, 129.7, 130.8, 135.8, 136.6, 150.9, 153.0, 162.9; mp (di-paratoluensulfonates salt) 199-201°C; MS (ESI$^+$) m/z = 735 (M +Na)$^+$. Anal.($C_{52}H_{56}N_4O_{16}S_2 \cdot 2H_2O$), C, H, N

2,7-Bis-[3-(3,4,5-trimethoxy-benzylamino)-propyl]-benzo[lmn][3,8] phenanthroline-1,3,6,8-tetraone (22): yellow oil; 85% yield; ^{1}H NMR (free base, 200 MHz, $CDCl_3$) δ 1.99-2.06 (m, 4H + 2H exchangeable with D_2O), 2.78 (t, 4H, J = 6.8), 3.77 (s, 4H), 3.82 (s, 6H), 3.87 (12H), 4.32 (t, 4H, J = 6.9), 6.59 (s, 4H), 8.74 (s, 4H); ^{13}C NMR (50 MHz, $CDCl_3$) δ 27.6, 38.4, 45.9, 49.7, 53.5, 55.6, 60.3, 104.5, 125.9, 126.0, 130.3, 135.2, 136.2, 150.6, 152.6, 162.3; mp (di-paratoluensulfonates salt) 199-201°C; MS (ESI$^+$) m/z = 741 (M +H)$^+$. Anal.($C_{54}H_{60}N_4O_{16}S_2 \cdot 2H_2O$), C, H, N

General Procedure for the Synthesis of 23-42:

A mixture of the appropriate diamine and the appropriate aldehyde (in a 1:5 molar ratio) in toluene was refluxed in a Dean-Stark apparatus for 5 h. Following solvent removal, the residue was taken up in EtOH, $NaBH_4$ (1:2.5 molar ratio) was added at 0 °C, and the stirring was continued at room temperature for 4 h. The solvent was then removed and the residue was dissolved in dichloromethane and washed with brine. Removal of the dried solvent gave a residue that was purified by flash chromatography using as eluent a mixture of dichloromethane/methanol/acqueous 33% ammonia (9:1:0.1), providing the desired products **23-42**.

***N*^{1}-(3-Methoxy-benzyl)-ethane-1,2-diamine (23):** yellow oil; 22% yield; ^{1}H NMR (free base, 400 MHz, $CDCl_3$) δ 1.74 (brs, 3H exchangeable with D_2O), 2.69 (t, 2H, J = 6), 2.81 (t, 2H, J = 5.6), 3.77 (s, 2H), 3.80 (s, 3H), 6.77-6.80 (m, 1H), 6.88-6.90 (m, 2H), 7.21-7.26 (m, 1H); ^{13}C NMR (100 MHz, $CDCl_3$) δ 41.3, 51.3, 53.5, 54.9, 112.1, 113.4, 120.2, 129.1, 141.8, 159.5.

***N*^{1}-(3-Methoxy-benzyl)-propane-1,3-diamine (24):** yellow oil; 60% yield; ^{1}H NMR (free base, 400 MHz, $CDCl_3$) δ 1.42 (brs, 3H exchangeable with D_2O); 1.61-1.75 (m, 2H), 2.68-2.84 (m, 4H), 3.79 (s, 2H), 3.83 (s, 3H), 6.78-6.83 (m, 1H), 6.90-6.93 (m, 2H), 7.22-7.30 (m, 1H); ^{13}C NMR (100 MHz, $CDCl_3$) δ 33.6, 40.5, 47.2, 54.0, 55.0, 113.4, 120.3, 129.3, 142.2, 151.1, 159.7.

***N*^{1}-(4-Methoxy-benzyl)-ethane-1,2-diamine (25):** yellow oil; 21% yield; ^{1}H NMR (free base, 200 MHz, $CDCl_3$) δ 1.53 (brs, 3H exchangeable with D_2O), 2.68-2.74 (m, 2H), 2.82-2.88 (m, 2H), 3.77 (s, 2H), 3.82 (s, 3H), 6.86-6.91 (m, 2H), 7.26-7.30 (m, 2H); ^{13}C NMR (50 MHz, $CDCl_3$) δ 41.7, 51.8, 53.3, 55.3, 113.8, 129.3, 132.7, 158.6.

***N*^{1}-(4-Methoxy-benzyl)-propane-1,3-diamine:** yellow oil; 51% yield; ^{1}H NMR (free base, 200 MHz, $CDCl_3$) δ 1.64-1.71 (m, 2H); 1.74 (brs, 3H exchangeable with D_2O), 2.67-2.82 (m, 4H), 3.74 (s, 2H), 3.81 (s, 3H), 6.85-6.90 (m, 2H), 7.23-7.27 (m, 2H); ^{13}C NMR (50 MHz, $CDCl_3$) δ 33.2, 40.3, 46.9, 53.3, 55.0, 113.6,129.2, 132.3,158.5.

***N*^{1}-Benzyl-ethane-1,2-diamine (27):** yellow oil; 22% yield; ^{1}H NMR (free base, 200 MHz, $CDCl_3$) δ 1.70 (brs, 3H exchangeable with D_2O), 2.69-2.74 (m, 2H), 2.81-2.86 (m, 2H), 3.82 (s, 2H), 7.30-7.36 (m, 4H); ^{13}C NMR (50 MHz, $CDCl_3$) δ 41.5, 51.6, 53.8, 127.0, 128.2, 128.4, 140.3.

***N*^{1}-Benzyl-propane-1,3-diamine (28):** yellow oil; 30% yield; ^{1}H NMR (free base, 200 MHz, $CDCl_3$) δ 1.55-1.63 (m, 2H + 3H exchangeable with D_2O), 2.65-2.73 (m, 2H), 2.84-2.89 (m, 2H), 3.9 (s, 2H), 7.28-7.36 (m, 4H).

***N*^{1}-(2-Chloro-benzyl)-ethane-1,2-diamine (29):** yellow oil; 25% yield; ^{1}H NMR (free base, 200 MHz, $CDCl_3$) δ 1.64 (brs, 3H exchangeable with D_2O), 2.80 (t, 2H, *J* = 5.4), 2.91 (t, 2H, *J* = 5.2), 3.99 (s, 2H), 7.30-7.48 (m, 4 H); ^{13}C NMR (50 MHz, $CDCl_3$) δ 41.8, 51.4, 52.0, 127.1, 128.5, 129.7, 130.4, 138.0, 151.1.

***N*^{1}-(2-Chloro-benzyl)-propane-1,3-diamine (30):** yellow oil; 35% yield; ^{1}H NMR (free base, 200 MHz, $CDCl_3$) δ 1.32-144 (m, 2H + 3H exchangeable with D_2O), 2.36-2.51 (m, 4H), 3.57 (s, 2H), 6.87-6.94 (m, 2H), 7.02-7.13 (m, 2H); ^{13}C NMR (50 MHz, $CDCl_3$) δ 33.3, 40.3, 47.0, 51.1, 126.6, 128.0, 129.2, 129.8,133.4, 137.7.

***N*^{1}-(2-Fluoro-benzyl)-ethane-1,2-diamine (31):** yellow oil; 29% yield; ^{1}H NMR (free base, 400 MHz, $CDCl_3$) δ 1.45 (brs, 3H exchangeable with D_2O), 2.68 (t, 2H, *J* = 6), 2.81 (t, 2H, *J* = 6), 3.85 (s, 2H), 7.00-7.05 (m, 1H), 7.08-7.12 (m, 1H), 7.20-7.26 (m, 1H), 7.32-7.36 (m, 1H); ^{13}C NMR (100 MHz, $CDCl_3$) δ 41.4, 46.8, 51.4, 115.1 (J(C,F) = 86.8), 123.8 (J(C,F) = 16), 127.1 (J(C,F) = 58), 128.4 (J(C,F) = 32.4), 130.1 (J(C,F) = 19.2), 162.15.

***N*^{1}-(2-Fluoro-benzyl)-propane-1,3-diamine (32):** yellow oil; 55% yield; ^{1}H NMR (free base, 400 MHz, $CDCl_3$) δ 1.63-1.70 (m, 2H), 2.09 (brs, 3H exchangeable with D_2O), 2.70 (t, 2H, *J* = 6.4), 2.80 (t, 2H, *J* = 6.8), 3.83 (s, 2H), 6.99-7.04 (m, 1H), 7.07-7.11 (m, 1H), 7.19-7.26 (m, 1H), 7.29-7.34 (m, 1H); ^{13}C NMR (100 MHz, $CDCl_3$) δ 32.9, 40.5, 47.3, 47.4, 115.3 (J(C,F) = 86.8), 124.2 (J(C,F) = 12.8), 127.2 (J(C,F) = 61.2), 128.8 (J(C,F) = 32.4), 130.5 (J(C,F) = 19.6), 160.1.

***N*^{1}-(2-Nitro-benzyl)-ethane-1,2-diamine (33):** yellow oil; 59% yield; ^{1}H NMR (free base, 400 MHz, $CDCl_3$) δ 1.71 (brs, 3H exchangeable with D_2O), 2.71 (t, 2H, J = 5.2), 2.83 (t, 2H, J = 5.8), 4.06 (s, 2H), 7.39-7.46 (m, 1H), 7.54-7.62 (m, 2H), 7.92-7.96 (m, 1H); ^{13}C NMR (100 MHz, $CDCl_3$) δ 41.8, 50.7, 52.0, 124.8, 128.0, 131.2, 133.1, 135.7, 147.8.

***N*^{1}-(2-Nitro-benzyl)-propane-1,3-diamine (34):** yellow oil; 35% yield; ^{1}H NMR (free base, 400 MHz, $CDCl_3$) δ 1.55-1.60 (m, 2H), 1.84 (brs, 3H exchangeable with D_2O), 2.59-2.74 (m, 4H), 3.94 (s, 2H), 7.28-7.36 (m, 1H), 7.49-7.52 (m, 2H), 7.81-7.85 (m, 1H); ^{13}C NMR (100 MHz, $CDCl_3$) δ 33.2, 40.4, 47.5, 50.9, 124.7, 127.9, 131.2, 133.1, 135.7, 149.2.

***N*^{1}-(2-Trifluoromethyl-benzyl)-ethane-1,2-diamine (35):** yellow oil; 67% yield; ^{1}H NMR (free base, 400 MHz, $CDCl_3$) δ 1.77 (brs, 3H exchangeable with D_2O), 2.73 (t, 2H, J = 6.2), 2.81 (t, 2H, J = 6.4), 3.96 (s, 2H), 7.28-7.65 (m, 4H); ^{13}C NMR (400 MHz, $CDCl_3$) δ 41.4, 49.7, 51.7, 125.7, 126.8, 127.3, 127.8, 128.4, 130.2, 131.8.

***N*^{1}-(2-Trifluoromethyl-benzyl)-propane-1,3-diamine (36):** yellow oil; 47% yield; ^{1}H NMR (free base, 200 MHz, $CDCl_3$) δ 1.54 (brs, 3H exchangeable with D_2O), 1.63-1.76 (m, 2H), 2.72-2.85 (m, 4H), 3.97 (s, 2H), 7.29-7.67 (m, 4H); ^{13}C NMR (100 MHz, $CDCl_3$) δ 31.3, 39.9, 47.4, 49.8, 125.7, 125.8, 126.9, 130.2, 131.9, 138.7.

***N*^{1}-(2-Methyl-benzyl)-ethane-1,2-diamine (37):** yellow oil; 23% yield; ^{1}H NMR (free base, 400 MHz, $CDCl_3$) δ 1.57 (brs, 3H exchangeable with D_2O), 2.72 (s, 3H), 2.72-2.75 (m, 2H), 2.81-2.84 (m, 2H), 3.77 (s, 2H), 7.14-7.17 (m, 3H), 7.26-7.30 (m, 1H); ^{13}C NMR (100 MHz, $CDCl_3$) δ 18.6 41.2, 51.1 51.7 125.5 126.5, 127.9 129.8, 135.8, 137.9.

***N*^{1}-(2-Methyl-benzyl)-propane-1,3-diamine (38):** yellow oil; 42% yield; ^{1}H NMR (free base, 200 MHz, $CDCl_3$) δ 1.58-1.64 (m 2H), 2.01 (brs, 3H exchangeable with D_2O), 2.29 (s, 3H), 2.64-2.75 (m, 4H), 3.69 (s, 2H), 7.09-7.14 (m, 3H), 7.21-7.24 (m, 1H);^{13}C NMR (100 MHz, $CDCl_3$) δ 17.6, 31.8, 38.9, 46.4, 50.4, 124.5, 125.5, 126.9, 128.8, 134.8, 137.2.

***N*^{1}-(2,3,4-Trimethoxy-benzyl)-ethane-1,2-diamine (39):** yellow oil; 88% yield; ^{1}H NMR (free base, 200 MHz, $CDCl_3$) δ 2.1 (brs, 3H exchangeable with D_2O), 2.66-2.75 (m, 2H), 2.84 (t, 2H, *J* = 5.3), 3.74 (s, 2H), 3.85-3.92 (m, 9H), 6.61-6.65 (d, 1H, *J* = 8.4), 6.94-6.98 (d, 1H, *J* = 8.4).

***N*^{1}-(2,3,4-Trimethoxy-benzyl)-propane-1,3-diamine (40):** yellow oil; 51% yield; ^{1}H NMR (free base, 200 MHz, $CDCl_3$) δ 1.61-1.71 (m, 2H), 2.09 (brs, 3H exchangeable with D_2O), 2.64 (t, 2H, *J* = 7.0), 2.75 (t, 2H, *J* = 6.6), 3.71 (s, 2H), 3.83-3.91 (m, 9H), 6.59-6.63 (d, 1H, *J* = 8.4), 6.9-6.94 (d, 1H, *J* = 8.8).

***N*^{1}-(3,4,5-Trimethoxy-benzyl)-ethane-1,2-diamine (41):** yellow oil; 82% yield; ^{1}H NMR (free base, 200 MHz, $CDCl_3$) δ 2.3 (brs, 3H exchangeable with D_2O), 2.68 (t, 2H, *J* = 5.4), 2.78 (t, 2H, *J* = 5.2), 3.67-3.80 (m, 11H), 6.52 (s, 2H); ^{13}C NMR (50 MHz, $CDCl_3$) δ 40.8, 50.9, 53.5, 55.5, 60.2, 104.4, 135.6, 136.2, 152.6.

***N*^{1}-(3,4,5-Trimethoxy-benzyl)-propane-1,3-diamine (42):** yellow oil; 91% yield; ^{1}H NMR (free base, 200 MHz, $CDCl_3$) δ 1.64(brs, 3H exchangeable with D_2O), 1.2-1.76 (m, 2H), 2.69 (t, 2H, *J* = 6.6), 2.81 (t, 2H, *J* = 7.0), 3.64 (s, 3H), 3.70 (s, 2H), 3.79 (s, 3H), 3.83 (s, 3H), 6.55 (s, 2H); ^{13}C NMR (50 MHz, $CDCl_3$) δ 31.0, 39.4, 46.4, 53.5, 55.7, 60.3, 104.7, 135.2, 136.3, 152.7.

(B) Biology. Growth-Inhibiting Activity. The NCI screening is a two-stage process,[19] beginning with the evaluation of all compounds against the 60 cell lines at a

single concentration of 10^{-5} M. Compounds exhibiting significant growth inhibition were evaluated against the 60-cell panel at five concentration levels by the NCI according to standard procedures (http://dtp.nci.nih.gov/branches/btb/ivclsp.html). In both cases the exposure time was 48 h.

Indirect immunofluorescence of cellular microtubules and Tubulin assembly inhibition assay.

Human A549 non small lung carcinoma cells were cultured in RPMI 1640 supplemented with 10% FCS, glutamine, and antibiotics as previously described.[41] Indirect immunofluorescence was performed in A549 cells that had been cultured overnight in 12 mm round coverslips and incubated a further 24 hours in the absence (drug vehicle DMSO) or in the presence of different ligand concentrations. Attached cells were permeabilized with Triton X100 and fixed with 3.7 % formaldehyde. Microtubules were specifically stained with DM1A α-tubulin monoclonal antibodies and DNA with Hoechst 33342 as previously described.[42] The preparations were examined using a Zeiss axioplan epifluorescence microscope and the images were recorded in a Hamamatsu 4742-95 cooled CCD camera.

The effect of the compounds in the assembly of purified tubulin was determined by incubating 25 μM purified tubulin at 37 ºC for 30 minutes in GAB (glycerol assembling buffer, 3.4 M glycerol, 10 mM sodium phospate, 1 mM EGTA, 1 mM GTP at pH 6.5) in the presence of 30 μM test compound, docetaxel, or podofilotoxin or 2 μL DMSO (vehicle). The samples were processed and the critical concentration for tubulin assembly[43] in the presence of the ligands calculated as described.[44]

Cell death assays. Cell culture and treatment: HeLa cells were cultured in HAM'S F-12 / MEM containing 10% fetal bovine serum, 5% glutamine, 1% non-essential amino acids and antibiotic solution. All tested compounds were dissolved in dimethylsulphoxide, diluted to at 1000x solution and added to cell cultures. Control cells received the corresponding volume of the vehicle. Cell viability was determined by trypan blue exclusion by counting living cells and stained dead cells with a Burker hemocytometer. Samples were done in triplicate, and at least 10 fields were counted for each sample. At the end of the incubation, once the number of living cells in samples were measured, cell survival was calculated as the percentage of living viable cells in treated samples in respect to the number of viable cells in control samples. The IC_{50} value is the concentration of toxic compound required to reduce cell survival to 50%.

The assays used to detect apoptosis were: caspase activation and nuclear morphology. The activity of Caspase protease enzymes was measured by the cleavage of the fluorogenic peptide substrate AcDEVD-AMC. At the indicated time points, cells were washed in phosphate-buffered saline, harvested in 0.4 ml of lysis buffer, and subjected to two cycles of freeze-thawing. The lysates were centrifuged for 10v min. at 28,000×g at 4°C and the supernatant was then used to assay in duplicate enzyme activity. Extract (10 µl) was incubated for 15 min at 37°C in a final volume of 30 µl to determine caspase activity.

The effect of treatments on nuclear morphology was determined by the visualization of 4',6-diamidino-2-phenylindole (DAPI)-stained nuclei. At the indicated time point, cells grown in triplicate on glass coverslips were washed twice with cold PBS, fixed in ice-cold methanol/acetic acid (1:1, v/v) for 15 min., rinsed with PBS, and then

stained with 0.1 mg/ml of DAPI. After staining, cells were mounted on standard glass slides and observed with a IX50 Olympus inverted microscope (Olympus, Tokyo, Japan). Apoptotic cells were identified by nuclear features characteristic of apoptosis (nuclear shrinkage and/or fragmentation, chromatin condensation).

Western blotting: Cells were collected in 5 mM dithiothreitol, 2 mM EDTA, 0.1% CHAPS, 0.1% Triton X-100, and protease inhibitors in 20 mM HEPES pH 7.5 and subjected to two cycles of freeze-thawing. The homogenate was then centrifuged at 15,000 × *g* for 15 min and the supernatant, diluted in loading buffer (2% SDS, 5% glycerol, 0.002% bromophenol blue, 4% β-mercaptoethanol in 0.25 M Tris–HCl, pH 6.8), and then denatured by boiling for 4 min. Aliquots corresponding to 80 µg protein were analyzed by SDS-PAGE. Proteins were transferred onto a nitrocellulose membrane and probed with the specific primary antibody. After further washing, the membrane was then incubated for 1h with peroxidase-conjugated goat anti-rabbit IgG (Santa Cruz). Immunoreactive bands were visualized by chemioluminescence with the ECL reagent (Amersham). Antibodies against total and phosphorylated ERK1/2 were from Cell Signaling. Anti actin was obtained from Santa Cruz. Actin was used as internal control.

DNA binding assays.

The binding to DNA was determined by a fluorometric ethidium displacement test at pH 8.[24, 25] The assay mixture contained 2 µg of ethidium bromide and 0.5 µg of calf thymus DNA in a final volume of 2 ml. Fluorescence (excitation at 525 nm; emission at 600 nm) was determined in triplicate following addition of aliquots of a 100x solution of polyamine compounds. The EC_{50} values are defined as the drug concentration which reduces the fluorescence of the DNA-bound ethidium by 50%.

Fluorescence melting assay. Fluorescence melting curves were determined in a Roche LightCycler (λecc 470 nm, λemm 520 nm) in LiP buffer (10 mM LiOH, 50 mM KCl, pH 7.4 with H_3PO_4). increasing ligands concentrations were added to 0.25 μM final concentration of a labelled human telomeric sequence (5'-Dabcyl-AGGGTTAGGGTTAGGGTTAGGGT-FAM 3', Eurogentec, Belgium). Before scan acquisition the reaction mixture was first denatured and annealed. Then, samples were maintained at 30° for 5 min before being slowly heated to 95 °C (1°C/ min) and annealed at a rate of 1°C/min. When double stranded DNA was used, dsUP (5'-FAM-ACTATTCCCGGGTAATGA) and dsDOWN (TCATTACCCGGGAATAGT-Dabcyl 3') were mixed at equimolar concentrations, heated to 95°C for 5 min, and then cooled to room temperature overnight before use. Recordings were taken during both the annealing and melting steps.

T_m values were determined from the first derivatives of the melting profiles using the Roche LightCycler software. Each curve was repeated at least three times and errors were ± 0.4°C.

Circular dichroism measurements. Circular dichroism spectra from 230 to 450 nm were recorded using 10 mm path length cells on a Jasco J 810 spectropolarimeter equipped with a NESLAB temperature controller and interfaced to a PC 100 in 10 mM Tris-HCl, 50 mM KCl pH 7.4. Experiments were performed by ligands to a solution of 4 μM Tel 22(5'-AGGGTTAGGGTTAGGGTTAGGG-3', Eurogentec, Belgium) or 45 μM ctDNA (Sigma). Before data acquisition, Tel22 solutions were heated at 95°C for 5 min and left to cool at room temperature o.n.. The reported spectrum of each sample represents the average of 3 scans recorded with 1-nm step

resolution. Observed ellipticities were converted to mean residue ellipticity [θ] = deg x cm^2 x $dmol^{-1}$ (Mol. Ellip.).

UV-VIS spectroscopic titrations. Spectrophotometric titrations were performed in 10 mM Tris-, 20 mM KCl, pH 7.5with a Perkin-Elmer Lambda 12 apparatus. Binding was followed by addition of increasing amounts of DNA to a freshly prepared drug solution. For each drug/DNA ratio the fraction of bound ligand was calculated ($\nu = (\varepsilon - \varepsilon_o)/(\varepsilon_\infty - \varepsilon_0)$, where ε_o and ε_∞ are the extinction coefficient of the free and DNA-bound ligand, respectively). To avoid large systematic inaccuracies due to experimental errors, the range of bound drug fractions utilized for calculations was 0.15-0.85. For titrations with ctDNA, data were evaluated according to the equation of McGhee and Von Hippel for non-coopative ligand-lattice interactions.[45] G-quadruoplex isotherms were analyzed according to a single set of identical sites.

***Taq* Polymerase Assay.** *Taq* polymerase reaction in the presence/absence of ligands and their metal complexes were performed using pBR322 (2.5 ng) as a DNA template and appropriate primer sequences Tup and Tdown (0.5 μM) to amplify the 906-1064 sequence of plasmid by PCR. The reaction was carried out in an Eppendorf thermocycler performing 25 cycles of: 30 s at 94°C, 30 s at 65 °C and 30 s at 72 °C. The reaction products were resolved on a 2% agarose gel in 1X TBE (89 mM Tris base, 89 mM boric acid, 2 mM Na_2EDTA) and stained by ethidium bromide.

Telomerase Activity Assay. 8 $x10^4$ HeLa cells in exponential phase of growth were seeded In a 6-wells plate. After 24h they were treated with increasing concentration of drug and incubated for further 24 h. Then, cells were pelleted and lysed for 30 min on ice using 100 μl of 0.5% CHAPS, 1 mM EGTA, 25% 2-mercaptoethanol, 1.74% PMSF and 10% w/v glycerol. The lysate was centrifuged at 13000 rpm for 30 min at 4

°C and the supernatant used as telomerase source. Telomerase activity was assayed using TRAPeze telomerase detection kit (Chemicon International). The reaction products were loaded onto a 10% polyacrylamide gel (19:1) in TBE 0.5X. Gels were stained with SbrGreen I.

In vitro screening in human tumor cell lines. Drug stock solutions (1×10^{-2} M) were prepared in cell culture DMSO. These were initially diluted in phosphate buffer saline (1×10^{-3} M) and finally in complete growth medium (1×10^{-4} M). Several µL were taken and put into cell culture plates to obtain different drug concentrations (highest final DMSO concentration was 0,05%). All controls contained the highest DMSO concentration used in the treated samples.

Cells were plated in 96-well tissue culture plates, allowed to attach 24 hours, and then left untreated or treated with growth medium containing 0.25, 0.50, 0.75, 1.0, 1.25, 1.5, 1.75, 2.0 µM **2**,**14**,**16**, or **18**. Briefly, fifteen µL of 5 mg/mL 3-(4,5-diphenyltetrazolium) bromide (MTT) in PBS were then added to each well and cells were incubated for 4 h at 37°C. Formazan crystals were made soluble with DMSO (all reagents were from Sigma-Aldrich (St. Louis, MO, USA). Optical densities were determined at 570 nm using a Dynatech MR5000 plate reader. Viability was expressed as a percentage of control by dividing the absorbance of each treated well by the average of the untreated controls. Cytotoxicity was determined by plotting cell viability versus drug concentrations. Results, derived from three different experiments, are expressed as mean percentage from quadruplicate wells as compared to that of control cells. The IC_{50} of the tested compounds were estimated graphically from the dose-response curves after 48 h of drug exposure.

Analysis of DNA synthesis by pulse labeling with bromodeoxyuridine. Exponentially growing neuroblastoma cells HTLA-230 were treated for 24 hours or 48 hours with 1.50 µM of **20**, pulse labelled with 10µM bromodeoxyuridine (BrdU; Sigma) for 1 hour, harvested by scraping, washed twice with 1 % bovine serum albumin (BSA) in PBS, and fixed with 70 % ice-cold ethanol for 30 minutes at 4°C. The cells were incubated for 30 minutes at room temperature in 2N HCl/0.5 % Triton X-100 to denature the DNA and to produce single-stranded molecules, then washed with 0.1 M $Na_2B_40_7$ (pH 8.5) to neutralize the acid, and resuspended in 0.5 % Tween 20/1 % BSA/PBS. BrdU uptake was detected by staining the cells with 20µL fluorescein isothiocynate (FITC)-conjugated mouse monoclonal anti-BrdU antibody (Becton Dickinson, Milan, Italy) at final concentration of 5 µg/mL for 30 minutes at room temperature. The cells were washed and resuspended in PBS containing 5 µg/mL propidium iodide (PI). Bivariate distributions of BrdU amounts (fluorescein isothiocynate, y-axis) versus DNA content (propidium iodide, x-axis) were assessed by flow cytometry using FACScan device (Beckton Dickinson) equipped with a xenon lamp and a filter set for excitation at 488 nm; FITC and PI fluorescence intensities were recorded through 520- to 530-nm and 575-nm filters, respectively. At least 100 000 cells were analyzed to produce each final densitometric plot. The gates represent the different phases of the cell cycle (R1 = sub-G_1 phase, R2 = G_1 phase, R3 = S phase, R4 = G_2/M phase).

Annexin V-FITC/PI stained fluorescence-activated cell sorter (FACS). To assess the effect of **20** on apoptosis, OVCAR 3.0 cells were stained with Annexin V-FITC/PI according to the manufacturer's instructions (Immunostep, S.L.; Salamanca, Spain). Briefly, adherent cells were plated at a concentration of 90 x 10^5 cells/well, 6-well

plate and after 24 h treated with **20** at 1.5, 2.0 or 2.5 μM. After 48 h or 72 h incubation cells were detached with scraper and washed twice with cold PBS and then suspended in 1x Binding Buffer at a concentration of 1 x 10^6 cells/mL. Hundred microliters of the suspension were transferred to a 5 mL tube and 5 μL of Annexin V-FITC and 5 μL of PI were added. The samples were gently vortexed and incubated for 15 min at 25°C in the dark. Finally, 400 μL of 1x Binding Buffer were added to each tube and the samples were analyzed by flow cytometry within 1 h at two wavelengths 515 and 639 nm. The used flow cytometer was a FACScan (Becton Dickinson) and the analysis was performed with Cell Quest software. Vehicle (DMSO) treated unstained and stained cells were used as controls.

Statistics

For the experiments involving *in vitro* drug treatment mean values and standard deviation for untreated and treated groups at different times were calculated. In addition, statistical significance of differences between untreated and treated groups at different times was determined by Mann-Whitney test., two tailed, with 95%confidence intervals using GraphPad Prism 3.0 software (GraphPad Software, Inc.).

Acknowledgment. This research was supported by a grant from MIUR, Rome (PRIN), University of Bologna (RFO) and Polo Scientifico-Didattico di Rimini (to V.T.). We thank the National Cancer Institute (Bethesda, MD) for the anticancer assays. MICINN (Spanish Government) is acknowledged for grant BIO2010-16351 (to J.F.D.). Lizzia Raffaghello is a recipient of MFAG Grant. Giovanna Bianchi is a recipient of a FIRC fellowship.

Supporting Information Available. Experimental details for chemistry, biology, characterization and elemental analyses of target compounds, and experimental details and characterization of intermediate compounds. This material is available free of charge via the Internet at http://pubs.acs.org.

References

1. Takenaka, S.; Takagi, M. Threading Intercalators as a New DNA Structural Probe. *Bulletin of the Chemical Society of Japan* **1999,** 72, 327-337.
2. Brana, M. F.; Cacho, M.; Gradillas, A.; de Pascual-Teresa, B.; Ramos, A. Intercalators as anticancer drugs. *Curr Pharm Des* **2001,** 7, 1745-80.
3. Martinez, R.; Chacon-Garcia, L. The search of DNA-intercalators as antitumoral drugs: what it worked and what did not work. *Curr. Med. Chem.* **2005,** 12, 127-51.
4. Tumir, L. M.; Piantanida, I. Recognition of single stranded and double stranded DNA/RNA sequences in aqueous medium by small bis-aromatic derivatives. *Mini Rev Med Chem* **2010,** 10, 299-308.
5. Strekowski, L.; Wilson, B. Noncovalent interactions with DNA: an overview. *Mutat Res* **2007,** 623, 3-13.
6. Nojima, T.; Ohtsuka, K.; Nagamatsu, T.; Takenaka, S. Bis-naphthalene diimide exhibiting an effective bis-threading intercalating ability. *Nucleic Acids Res Suppl* **2003**, 123-4.
7. Gianolio, D. A.; McLaughlin, L. W. Tethered naphthalene diimide intercalators enhance DNA triplex stability. *Bioorg Med Chem* **2001,** 9, 2329-34.
8. Balasubramanian, S.; Neidle, S. G-quadruplex nucleic acids as therapeutic targets. *Curr Opin Chem Biol* **2009,** 13, 345-53.
9. Di Antonio, M.; Doria, F.; Richter, S. N.; Bertipaglia, C.; Mella, M.; Sissi, C.; Palumbo, M.; Freccero, M. Quinone methides tethered to naphthalene diimides as selective G-quadruplex alkylating agents. *J Am Chem Soc* **2009,** 131, 13132-41.
10. Gunaratnam, M.; Swank, S.; Haider, S. M.; Galesa, K.; Reszka, A. P.; Beltran, M.; Cuenca, F.; Fletcher, J. A.; Neidle, S. Targeting human gastrointestinal stromal tumor cells with a quadruplex-binding small molecule. *J Med Chem* **2009,** 52, 3774-83.
11. Liu, Z. R.; Hecker, K. H.; Rill, R. L. Selective DNA binding of (N-alkylamine)-substituted naphthalene imides and diimides to G+C-rich DNA. *J. Biomol. Struct. Dyn.* **1996,** 14, 331-9.
12. Tumiatti, V.; Milelli, A.; Minarini, A.; Micco, M.; Gasperi Campani, A.; Roncuzzi, L.; Baiocchi, D.; Marinello, J.; Capranico, G.; Zini, M.; Stefanelli, C.; Melchiorre, C. Design, synthesis, and biological evaluation of substituted naphthalene imides and diimides as anticancer agent. *J Med Chem* **2009,** 52, 7873-7.
13. Schneider, H. J. Ligand binding to nucleic acids and proteins: Does selectivity increase with strength? *Eur J Med Chem* **2008,** 43, 2307-15.
14. Tumiatti, V.; Rosini, M.; Bartolini, M.; Cavalli, A.; Marucci, G.; Andrisano, V.; Angeli, P.; Banzi, R.; Minarini, A.; Recanatini, M.; Melchiorre, C. Structure-activity relationships of acetylcholinesterase noncovalent inhibitors based on a polyamine backbone. 2. Role of the substituents on the phenyl ring and nitrogen atoms of caproctamine. *J Med Chem* **2003,** 46, 954-66.
15. Cavalli, A.; Bolognesi, M. L.; Minarini, A.; Rosini, M.; Tumiatti, V.; Recanatini, M.; Melchiorre, C. Multi-target-directed ligands to combat neurodegenerative diseases. *J Med Chem* **2008,** 51, 347-72.
16. Petrelli, A.; Valabrega, G. Multitarget drugs: the present and the future of cancer therapy. *Expert Opinion on Pharmacotherapy* **2009,** 10, 589-600.

17. Hagmann, W. K. The many roles for fluorine in medicinal chemistry. *J Med Chem* **2008,** 51, 4359-69.
18. Grever, M. R.; Schepartz, S. A.; Chabner, B. A. The National Cancer Institute: cancer drug discovery and development program. *Semin Oncol* **1992,** 19, 622-38.
19. Monks, A.; Scudiero, D.; Skehan, P.; Shoemaker, R.; Paull, K.; Vistica, D.; Hose, C.; Langley, J.; Cronise, P.; Vaigro-Wolff, A.; et al. Feasibility of a high-flux anticancer drug screen using a diverse panel of cultured human tumor cell lines. *J Natl Cancer Inst* **1991,** 83, 757-66.
20. Weinstein, J. N.; Myers, T. G.; O'Connor, P. M.; Friend, S. H.; Fornace, A. J., Jr.; Kohn, K. W.; Fojo, T.; Bates, S. E.; Rubinstein, L. V.; Anderson, N. L.; Buolamwini, J. K.; van Osdol, W. W.; Monks, A. P.; Scudiero, D. A.; Sausville, E. A.; Zaharevitz, D. W.; Bunow, B.; Viswanadhan, V. N.; Johnson, G. S.; Wittes, R. E.; Paull, K. D. An information-intensive approach to the molecular pharmacology of cancer. *Science* **1997,** 275, 343-9.
21. Lavrik, I. N.; Golks, A.; Krammer, P. H. Caspases: pharmacological manipulation of cell death. *J Clin Invest* **2005,** 115, 2665-72.
22. Robertson, J. D.; Orrenius, S.; Zhivotovsky, B. Review: nuclear events in apoptosis. *J Struct Biol* **2000,** 129, 346-58.
23. Balmanno, K.; Cook, S. J. Tumour cell survival signalling by the ERK1/2 pathway. *Cell Death Differ* **2009,** 16, 368-77.
24. Morgan, A. R.; Lee, J. S.; Pulleyblank, D. E.; Murray, N. L.; Evans, D. H. Review: ethidium fluorescence assays. Part 1. Physicochemical studies. *Nucleic Acids Res* **1979,** 7, 547-69.
25. McConnaughie, A. W.; Jenkins, T. C. Novel acridine-triazenes as prototype combilexins: synthesis, DNA binding, and biological activity. *J Med Chem* **1995,** 38, 3488-501.
26. LigPrep, version 2.3. In Schroedinger LLC: New York, 2009.
27. Mohamadi, F.; Richards, N. G. J.; Guida, W. C.; Liskamp, R.; Lipton, M.; Caufield, C.; Chang, G.; Hendrickson, T.; Still, W. C. Macromodel - an Integrated Software System for Modeling Organic and Bioorganic Molecules Using Molecular Mechanics. *Journal of Computational Chemistry* **1990,** 11, 440-467.
28. Mcdonald, D. Q.; Still, W. C. Amber-Asterisk Torsional Parameters for the Peptide Backbone. *Tetrahedron Letters* **1992,** 33, 7743-7746.
29. Hasel, D.; Hendrickson, T. F.; Still, W. C. A rapid approximation to the solvent accessible surface areas of atoms. *Tetrahedron Comput. Methodol.* **1988,** 1, 103-116.
30. Berman, H. M.; Westbrook, J.; Feng, Z.; Gilliland, G.; Bhat, T. N.; Weissig, H.; Shindyalov, I. N.; Bourne, P. E. The Protein Data Bank. *Nucleic Acids Res* **2000,** 28, 235-42.
31. Canals, A.; Purciolas, M.; Aymami, J.; Coll, M. The anticancer agent ellipticine unwinds DNA by intercalative binding in an orientation parallel to base pairs. *Acta Crystallogr D Biol Crystallogr* **2005,** 61, 1009-12.
32. Parkinson, G. N.; Cuenca, F.; Neidle, S. Topology conservation and loop flexibility in quadruplex-drug recognition: crystal structures of inter- and intramolecular telomeric DNA quadruplex-drug complexes. *J Mol Biol* **2008,** 381, 1145-56.

33. Alcaro, S.; Ortuso, F.; Coleman, R. S. DNA cross-linking by azinomycin B: Monte Carlo simulations in the evaluation of sequence selectivity. *J Med Chem* **2002,** 45, 861-70.
34. Morris, G. M.; Goodsell, D. S.; Halliday, R. S.; Huey, R.; Hart, W. E.; Belew, R. K.; Olson, A. J. Automated docking using a Lamarckian genetic algorithm and an empirical binding free energy function. *Journal of Computational Chemistry* **1998,** 19, 1639-1662.
35. Alcaro, S.; Gasparrini, F.; Incani, O.; Caglioti, L.; Pierini, M.; Villani, C. "Quasi flexible" automatic docking processing for studying stereoselective recognition mechanisms, part 2: Prediction of Delta Delta G of complexation and H-1-NMR NOE correlation. *Journal of Computational Chemistry* **2007,** 28, 1119-1128.
36. Alcaro, S.; Gasparrini, F.; Incani, O.; Mecucci, S.; Misiti, D.; Pierini, M.; Villani, C. A "quasi-flexible" automatic docking processing for studying stereoselective recognition mechanisms. Part I. Protocol validation. *Journal of Computational Chemistry* **2000,** 21, 515-530.
37. Alcaro, S.; Artese, A.; Iley, J. N.; Missailidis, S.; Ortuso, F.; Parrotta, L.; Pasceri, R.; Paduano, F.; Sissi, C.; Trapasso, F.; Vigorita, M. G. Rational Design, Synthesis, Biophysical and Antiproliferative Evaluation of Fluorenone Derivatives with DNA G-Quadruplex Binding Properties. *Chemmedchem* **2010,** 5, 575-583.
38. Alcaro, O.; Costa, G.; Distinto, S.; Moraca, F.; Ortuso, F.; Parrotta, L.; Artese, A. The polymorfism of DNA G-Quadruplex investigated by Docking Experiments with Telemestatin Enantiomers. *Curr. Pharm. Des*. **2011,** accepted.
39. Wolber, G.; Langer, T. LigandScout: 3-d pharmacophores derived from protein-bound Ligands and their use as virtual screening filters. *Journal of Chemical Information and Modeling* **2005,** 45, 160-169.
40. Alcaro, S.; Artese, A.; Iley, J. N.; Maccari, R.; Missailidis, S.; Ortuso, F.; Ottana, R.; Ragazzon, P.; Vigorita, M. G. Tetraplex DNA specific ligands based on the fluorenone-carboxamide scaffold. *Bioorganic & Medicinal Chemistry Letters* **2007,** 17, 2509-2514.
41. Buey, R. M.; Calvo, E.; Barasoain, I.; Pineda, O.; Edler, M. C.; Matesanz, R.; Cerezo, G.; Vanderwal, C. D.; Day, B. W.; Sorensen, E. J.; Lopez, J. A.; Andreu, J. M.; Hamel, E.; Diaz, J. F. Cyclostreptin binds covalently to microtubule pores and lumenal taxoid binding sites. *Nat Chem Biol* **2007,** 3, 117-25.
42. de Ines, C.; Leynadier, D.; Barasoain, I.; Peyrot, V.; Garcia, P.; Briand, C.; Rener, G. A.; Temple, C., Jr. Inhibition of microtubules and cell cycle arrest by a new 1-deaza-7,8-dihydropteridine antitumor drug, CI 980, and by its chiral isomer, NSC 613863. *Cancer Res* **1994,** 54, 75-84.
43. Oosawa, F. A., S. *Thermodynamics of the Polymerization of Proteins*. London, 1975.
44. Buey, R. M.; Barasoain, I.; Jackson, E.; Meyer, A.; Giannakakou, P.; Paterson, I.; Mooberry, S.; Andreu, J. M.; Diaz, J. F. Microtubule interactions with chemically diverse stabilizing agents: thermodynamics of binding to the paclitaxel site predicts cytotoxicity. *Chem Biol* **2005,** 12, 1269-79.
45. McGhee, J., von Hippel, P. . Theoretical aspects of DNA-protein interactions: co-operative and non co-operative binding of large ligands to a one-dimensional homogeneous lattice. *Journal of Molecular Biology* **1974,** 86, 469-489.

Table of Contents Graphic

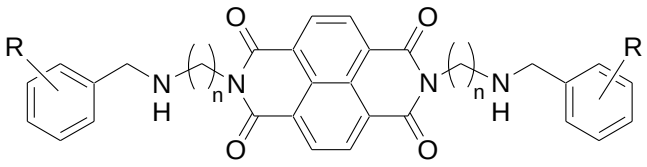

n = 2-3